Asia Pacific Research Initiative for Sustainable Energy Systems 2018 (APRISES18)

Office of Naval Research
Grant Award Number N00014-19-1-2159

Ocean Thermal Energy Conversion (OTEC) Heat Exchanger Development (August 2022 to May 2023)

Task 6

Prepared for
Hawai‘i Natural Energy Institute

Prepared by
Makai Ocean Engineering

June 2023

HNEI
Hawai‘i Natural Energy Institute
University of Hawai‘i at Mānoa

MAKAI OCEAN ENGINEERING

ANNUAL REPORT

Prepared For

HAWAII NATURAL ENERGY INSTITUTE

1680 East West Road, POST 109

Honolulu, HI, 96822

USA

Prepared By

MAKAI OCEAN ENGINEERING

PO Box 1206, Kailua, Hawaii 96734

June 28, 2023

TABLE OF CONTENTS

LIST OF FIGURES

LIST OF TABLES

1. INTRODUCTION

Makai Ocean Engineering has been developing Thin Foil Heat Exchangers (TFHX) for use in seawater-refrigerant, air-water, and water-water applications. This report summarizes work performed between August 2022 – May 2023.

In this period, Makai's efforts included introduction of new TFHX designs; implementation of weld defect identification and repair method; continued characterization of TFHX thermal and structural/mechanical performance, and initiation of biofouling mitigation methods.

TFHX Design

Makai introduced two new designs, one intended for seawater application with a different form factor (TFPX) and a pass-through design intended for air cooling (TFAC). Makai also established operating ranges and sizes for the existing modular design.

TFHX Fabrication

Makai completed the disassembly and re-assembly of the High Speed Welding Station (HSWS) and move to the new Fabrication Lab. With this move, all fabrication equipment is located in the same room and efficiency has been improved by having all the process steps in the same room.

Makai also developed and implemented a weld defect identification and repair system which has improved plate fabrication success rates from 50% to 77%. Makai will continue to improve the algorithm and repair techniques.

TFHX Performance

Makai developed additional pattern designs for seawater-ammonia testing, including varying the internal channel size across a plate and adding features to improve ammonia convection. Makai conducted seawater-ammonia performance tests on seven variations of the modular 4-port TFHX design. Makai also tested the new TFPX and TFAC designs.

TFHX Characterization

Makai's characterization efforts were focused on better understanding the parameters that affect fatigue life. Makai identified a fabrication step that led to a 3X increase in fatigue life.

Biofouling

Makai established a baseline for biofouling performance of an untreated module in warm seawater and evaluated the efficacy of a commercially available biofouling mitigation device. Makai also designed, constructed, and started testing on the first manual cleaning prototype. Initial results indicate that the biofouling control methods have delayed the onset of biofouling-induced performance degradation, but have not successfully eliminated or mitigated performance impacts caused by biofouling.

2. TFHX DESIGN

In this period, Makai's TFHX design efforts focused on developing two new TFHX designs, one for applications requiring both fluids to be enclosed and one for applications where the heat exchanger is immersed in the external fluid. Makai also tested the previously designed modular housings to establish operational pressure limits.

2.1. THIN-FOIL PIPE HEAT EXCHANGER (TFPX)

Makai previously developed a modular, four-port design for applications which used plate-frame style heat exchangers. However, some limitations of existing plate-frame heat exchangers were also present in the four-port modular design: 1) increased external fluid pressure drop associated with two 90° turns, 2) end plates must be used to contain external pressure, and 3) lack of easy access to clean the plates. Makai developed the Thin-Foil Pipe Heat Exchanger (TFPX) for applications in which the limitations of the four-port design can be an obstacle to adoption of the TFHX.

In the TFPX, thin foil plates are housed in a pipe which is a naturally efficient geometry to contain the external pressure. Each plate in the stack has a slightly different width to match the width of pipe cross section. The plates are stacked between clamping plates which hold the stack in compression and the assembly is inserted into the pipe as a unit. Flange connections are also used to connect to the external fluid which has a straight through flow path through the heat transfer section but must flow around the manifolds at the entrance and exit. Depending on the requirements of the application, multiple TFPX units could be arranged such that the external fluid flows through subsequent units in series or in parallel.

Makai designed two TFPX versions, one to fit in a 6" and the other a 12" Schedule 40 PVC pipe. Plates for the 6" TFPX can be fabricated using the mid-length welding fixture in which the manifold openings are 496 mm apart (center-to-center). At 2-mm plate spacing, the 6" TFPX has a stack of 50 plates totaling 5.475 m^2 of heat transfer area which is approximately half of a four-port module (which has double the plate length). The 12" TFPX unit holds 55 full-length plates (1-m long) at 4.12-mm plate spacing resulting in 23.8 m^2 of heat transfer area.

For applications that have the space and ability to stop water flows for cleaning, plates can be removed from the pipe as a stack and pressure washed or brushed for cleaning and reinstalled without having to disassemble the plate stack, which is a key difference between the four-port TFHX design and existing plate-frame heat exchangers. In the TFPX, the plate stack is removed from the housing as one unit and maintained under compression so the gaskets remain in place.

Figure 1. 6” TFPX prototype showing the housing and the plate stack.

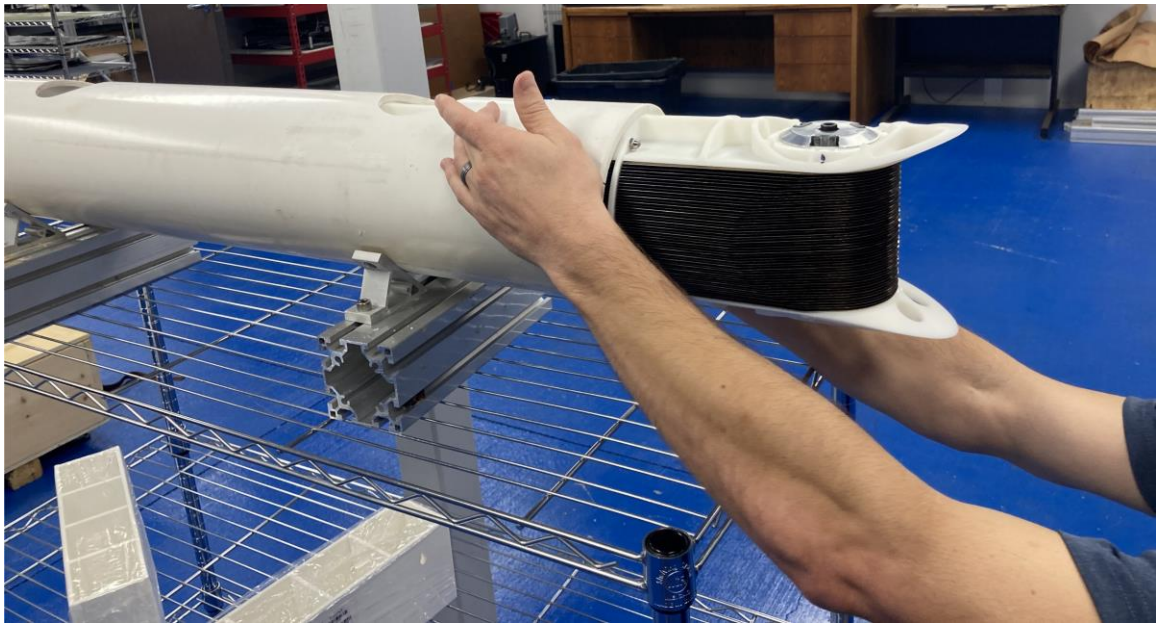

Figure 2. Inserting TFPX plate stack into pipe.

Makai constructed two 6” TFPX prototypes (Figure 1 and Figure 2) and conducted a seawater-seawater performance test on one unit (Section 4.2).

2.2. THIN-FOIL AIR CONDITIONER (TFAC)

In the modular four-port design, the module housing increases both the external fluid pressure drop and the overall cost of the unit. For applications in which the heat exchanger can be immersed in the external fluid (i.e., that do not require the external fluid to be encapsulated/enclosed), a pass-through design can be used to minimize the external pressure drop and reduce some of the overall cost.

Makai previously initiated a case study with Cyanotech and provided a pass-through TFHX prototype to cool the algae ponds using cold seawater. In this period, based on interest from NELHA and Blue Ocean Mariculture (BOM), Makai adapted the pass-through design into the Thin-Foil Air Conditioning (TFAC) unit which uses an off-the-shelf box fan and cold seawater to provide cooling and dehumidification for environmental control (Figure 3). Currently BOM is using diesel generators to power split A/C units for cooling. NELHA is also interested in using the TFAC to cool the pump room at the 55" pump station which has high heat loads from the pump VFDs. The current AC units must be replaced every 1-2 years due to corrosion issues in the marine air. The TFAC's titanium plates are not expected to have any corrosion issues and the box fan is treated as a widely available, easily replaceable, and economical consumable part.

In the TFAC, the cold seawater and air are arranged in a crossflow configuration. A single unit contains 20 plates or 6 m^2 of heat transfer area. Individual plates are constructed using the existing 55-mm manifold inserts and mid-length fixturing. Plates are compressed between two end plates and held in compression using threaded rods and nuts. Top and bottom covers complete the air duct. The bottom cover also includes a drip pan and drain to manage condensation.

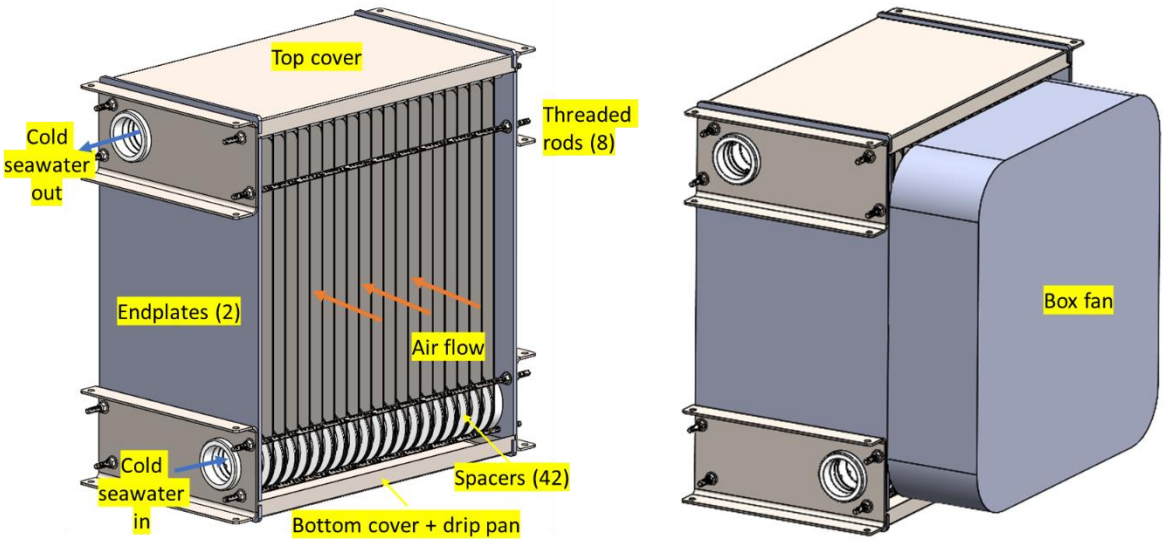

Figure 3. TFAC prototype using previously purchased spacers.

2.3. FULL-LENGTH, MODULAR, FOUR-PORT TFHX

Makai continues to fabricate and performance test (at the 100-kW scale) the four-port modular TFHX. In this period, Makai constructed and tested 7 design variations (Table 1). Performance testing results are discussed separately in Section 4.3.

Table 1. Overview of full-length configurations tested to date.

	Previous		
	TFHX-FL1	**TFHX-FL2**	**TFHX-FL3**
Plate Spacing [mm]	2.12	2.12	4.24
HX Area [m2]	10.32	10.32	5.16
Internal Channel Size [mm]	0.589	0.9	0.9
External Channel Size [mm]	1.275	0.964	3.082
Test configurations	e,c,w	e,c,w	e,c,w

	New this period						
	TFHX-FL4	**TFHX-FL5**	**TFHX-FL6**	**TFHX-FL7**	**TFHX-FL8**	**TFHX-FL9**	**TFHX-FL10**
Plate Spacing [mm]	2.12	2.12	4.24	2.12	4.24	2.12	2.12
HX Area [m2]	10.32	5.16	2.58	5.16	2.58	5.16	5.16
Internal Channel Size [mm]	0.78	0.78	0.78	0.503	0.5616	0.56	0.838
External Channel Size [mm]	1.084	1.084	3.202	1.361	3.421	1.304	1.026
Test configurations	e,c	e,c	e,c	e,c	e	e,c	e,c

Thermal and hydraulic performance are used to determine the number of modules required for a specific application. Makai designed the modules such that up to 16 modules could be stacked together to form one unit. For demonstration purposes Makai stacked a 9-module TFHX unit (Figure 4).

Figure 4. Demonstration of 9 modules stacked to form one full-length 4-port TFHX unit.

Another important consideration is the external fluid operating pressure. The module housing and the endplates determine the pressure rating for the external fluid. The module housings were designed to 100 psig, which means a pressure rating of 50 psig with a safety factor of 2. Two tests were conducted to verify the 100 psig burst pressure. For both tests, two modules were filled with full-length plates of varying designs and installed between endplates. The internal and external sides were filled and pressurized with water. A pressure sensor was installed on the external manifold to monitor pressure during the test. The external side was pressurized until failure.

In the first test, the external side was pressurized to 50 psig and held for a minute before continuing to pressurize to 100 psig. The module failed before reaching 60 psig. A section of the module blew out at ~59 psig. In the second test, the unit was first pressurized to 32 psig and held for over an hour without leaks prior to pressurizing to 50 psig. The unit held 50 psig for at least 24 minutes, but when re-checked after 1 hour, a leak was observed. Data recording was unavailable during the 50 psig hold.

The results of both tests were surprising. Makai had designed the housing to withstand 100 psig and intended to rate the modular TFHX units for 50 psig external operating pressure. Based on the test results, the pressure rating must be downgraded to 25 psig operating pressure to maintain a 2X safety factor.

The manufacturer suggested the failures may be occurring along a knit line, where two streams of plastic meet in the injection molding process, and a possible solution is to modify the mold to shift the knit lines to a lower stress location on the housing. At this point, since there are currently no

applications requiring a high pressure external fluid for the modular TFHX, Makai is not actively pursuing module modifications.

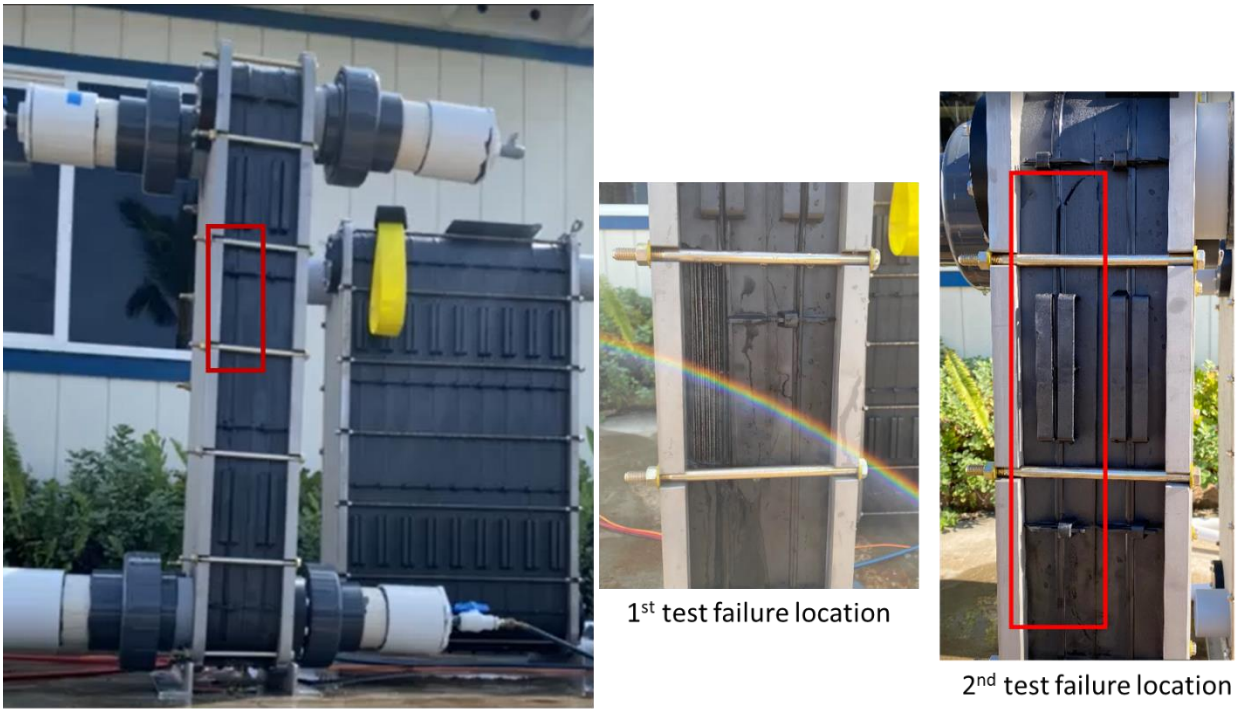

Figure 5. Module pressure test setup and failure locations for each of two tests.

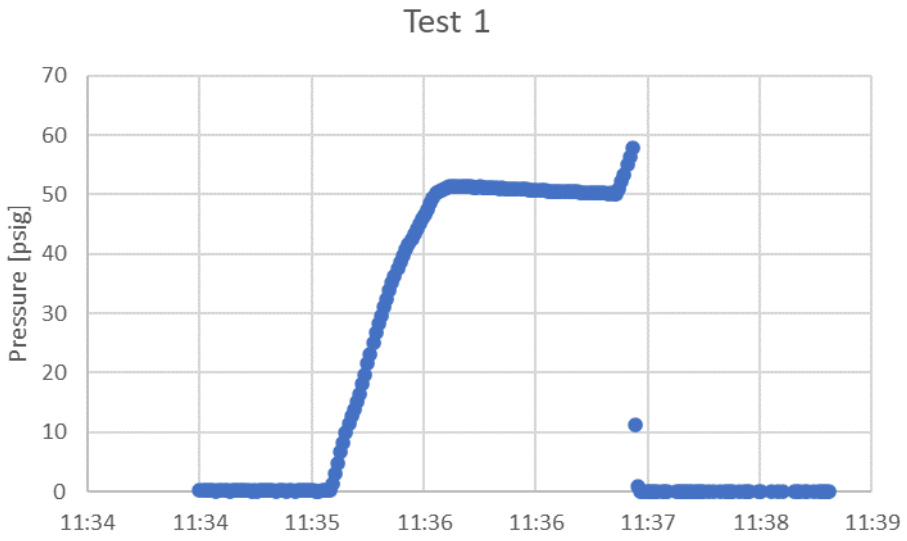

Figure 6. External pressure during first test. The module housing failed at 59 psig.

2.4. MATERIAL COMPATIBILITY

Makai previously reported success welding 0.002” and 0.003” stainless steel foil. Makai constructed a unit intended for air-water performance testing using 0.002” 316L stainless steel foil, pressure tested each plate with soap-bubble water spray, and let the plates sit on a shelf while waiting for the test assembly parts to arrive. The parts arrived after 1 month and Makai assembled the unit but the unit was unable to pass pressure testing. Upon inspection, multiple plates had pits that essentially left a hole in the plate (Figure 7).

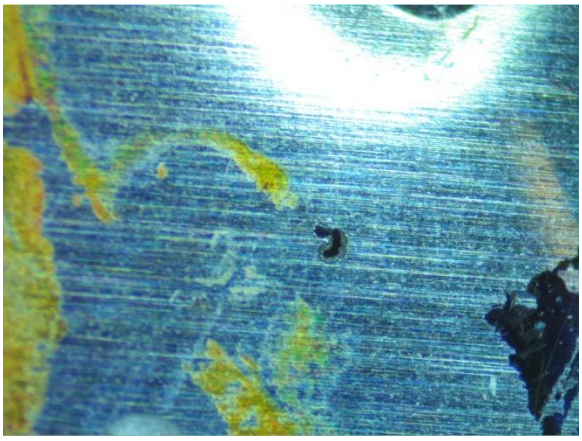

Figure 7. Pit in 0.002” SS316L foil along with rust spots.

Makai was able to construct a second unit out of 0.002” 316L for immediate testing and that unit did not have any corrosion issues. Unfortunately, with such thin foil any error in material quality or surface contamination will lead to catastrophic failure. For this reason, Makai has decided to stop pursuing 0.002” 316L as a cost-effective alternative to titanium.

3. TFHX FABRICATION

Makai focused fabrication efforts on improving efficiency and success rates to achieve fast, reliable, repeatable, high-quality TFHX plates. This includes revisions to improve existing equipment and fixturing and tooling and methods to improve weld quality control and repair.

Makai decided to move the HSWS to the newer Fabrication Laboratory. The HSWS was re-assembled and re-commissioned in the new space in July 2022. The new lab has better environmental controls (less humidity, less dust) and with the move, all production equipment for full-length plates is located in the same room. The consolidation of all equipment in the same location is an immediate improvement in fabrication efficiency since one person can perform multiple steps simultaneously.

After the move, plate success rates improved slightly but were still too low for commercial-scale heat exchanger production to be cost and resource effective. TFHX economics can be improved by both increasing the plate success rate and process improvements that result in lower cost components or faster production times.

In this period, Makai focused on:

- Troubleshooting plate failures and identifying fixturing-related issues,
- New fixturing to reduce per plate forming cost, and
- Quality control methods to identify and repair bad welds such that the majority of plates are usable (i.e., pressure rating and performance are comparable to a plate with no weld defects).

3.1. FABRICATION CHALLENGES

In this period, Makai experienced a series of plate failures that involved multiple issues which happened to occur at the same time. The series of failures began around the same time Makai switched to a new batch of foil that was procured from a new vendor. The main issues were repeated weld delamination failures and a burning smell accompanied by increased particulates (soot) after welding. These issues were isolated to separate fixturing issues which have been resolved.

3.2. FOIL FORM FIXTURE

In the current fabrication process, Makai purchases Grade 1 Titanium foil and sends it to a vendor to form the coil of foil into individual pieces. Originally, two steps (hits) were required to form the features, which is labor intensive. A new die set has been designed to form all features in a single step. Makai recently ordered the tooling and an initial set of plates and anticipates receiving the plates in the next month or two. If successful, the foil forming costs will be reduced by half.

3.3. QUALITY CONTROL

Control of fabrication environment is one way to improve the weld success rate. A second method is to identify and repair defective welds, to produce an overall successful plate. Makai's efforts in quality control were focused on improving plate success rates. Makai has classified four main types of plate failures:

- Weak welds: Multiple factors, such as contamination, lack of contact, insufficient shielding, or deviation from target power or time, may produce weak welds with poor adhesion
- Burn-throughs: A burn through creates a hole in the foil. Burn throughs are usually caused by lack of foil contact, contamination, or incompatible weld parameters. Burn-throughs can catalyze a string of successive failures because they can result in further loss of contact or lack of shielding.
- Pin-hole leaks: Unlike a burn-through which can cause a chain of failures, pinhole leaks are very small, localized leaks that are typically capable of holding some pressure but with a small leak rate. Some pinhole leaks are identifiable prior to expansion.
- Micro-cracks: Similar to pinhole leaks, a plate with a microcrack may reach full expansion pressure but a leak is detected during the final pressure check. Unlike pinhole leaks, microcracks are often undetectable until pressure testing.

The first step in quality control is to establish methods to identify defective welds. Makai's weld quality program uses high-resolution imaging and machine vision/machine learning to identify weld defects in real-time. Additionally, in order for the system to be effective, the system must be able to identify bad welds, but must also do so without significant impact to fabrication speed; otherwise, the TFHX would not be cost competitive.

In the early stages of algorithm development, welding was stopped whenever a bad weld was detected. This allowed time for the operator to assess whether the weld was actually bad or the algorithm flagged a false positive before continuing to weld repair. Over time, with machine learning and algorithm advances, the operator feedback step was eliminated and the system automatically repaired any welds identified as bad. Automating the imaging, identification, and repair added negligible time to the overall fabrication time.

3.4. ULTRA SPEED WELDING SYSTEM

The ultra-speed welding system (USWS) concept was developed as a production-scale solution to fabricate TFHX plates. In USWS, the foil is utilized directly from the coil, eliminating the forming step currently performed by a supplier. Re-designing the fabrication equipment to utilize raw coils of foil eliminates unwanted residual stresses associated with formed features and, as a result, is anticipated to improve foil contact and weld success rates. Furthermore, the forming step requires a custom form for each plate size/shape and the corresponding fixturing to hold the formed foil pieces in the HSWS. While there are few theoretical design limitations to TFHX shapes or sizes, the custom fixturing required to fabricate in the HSWS imposes practical cost limitations. The

USWS concept eliminates the need for custom fixturing and enables more rapid prototyping for different plate shapes and sizes.

3.5. ECONOMIC ANALYSIS

Categories that contribute to TFHX cost include: materials/components (e.g., foil, inserts, o-rings), labor, heat exchanger components (e.g., modules, endplates, hardware), consumables, and overhead. Previously, Makai's focus was on reducing material costs to make the TFHX cost competitive. In this period, Makai's focus has been on reducing the plate costs by improving plate success rates and reducing fabrication time.

In this period, Makai's efforts reduced TFHX plate costs by 40% and the overall TFHX unit cost by 35%.

Compared to previous TFHX versions, the current 4-port, full-length TFHX costs includes module housings, endplates, and overhead which were not accounted for in 3B, 3C, and 3E. Even with the added cost categories, Makai has made a 5X reduction in $/m2 from the original 3B design to the current 4-port, full-length TFHX.

The heat exchanger component contribution to the overall TFHX cost depends on the number of modules in a TFHX unit. Two module halves are required for every 24 plates and a set of end plates and hardware are required for every unit. A unit can be as small as one single module or up to 16 modules. In terms of $/m^2, it is more cost effective to have 16 modules in a unit; the endplate costs are distributed over 16 modules instead of a single module. This current economic analysis is based on using 16 modules (165 m^2 of heat transfer area) per unit, which is comparable to the heat transfer area of previously purchased 2-MW scale plate-frame (205-277 m^2), brazed-fin (135 m^2), and shell-and-tube heat exchangers (164-179 m^2).

Compared to commercially available heat exchangers, the latest iteration of the 4-port TFHX is cost competitive, particularly when considering the TFHX's titanium material and compact form factor (Figure 8). Commercial heat exchanger costs are based on heat exchanger areas ~1000/m^2 and mature production lines. Makai's TFHX is still fabricated in on an R&D platform with highly skilled labor. With planned advancements in quality control and improvements in fabrication equipment, Makai expects the TFHX will be the more cost effective option when compared to titanium plate-frame heat exchangers.

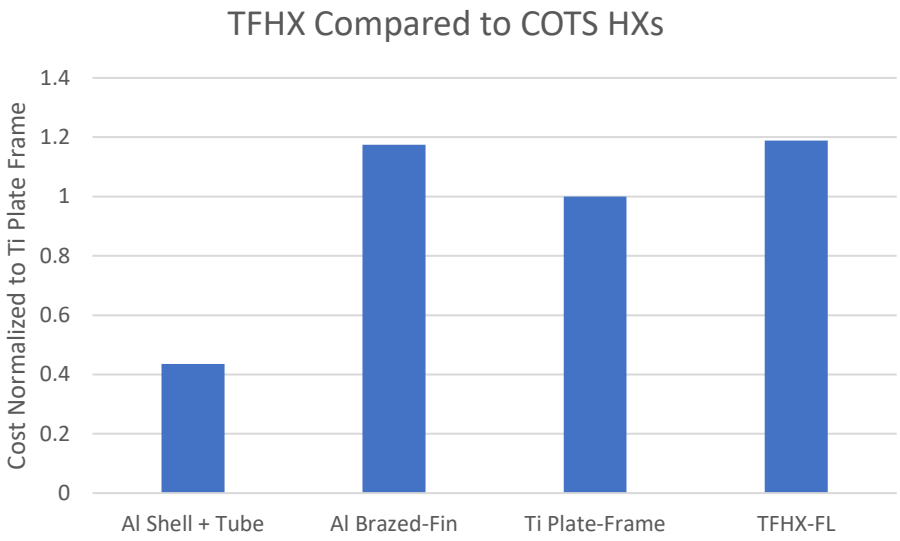

Figure 8. TFHX costs compared to COTS heat exchangers.

4. TFHX PERFORMANCE TESTING

4.1. AIR-WATER TFAC TESTING

Makai constructed and tested a TFAC unit outdoors first and then indoors in the corrosion lab (Figure 9). In the initial unit, the fan was from a window air conditioning unit and makeshift air ducting using cardboard was used to ensure air flow was directed between the plates. The second indoor test used a box fan and corrugated board ducting. Cold seawater was supplied to the inside of the plates. Cold seawater and air inlet/outlet temperatures and cold seawater flow rates were measured.

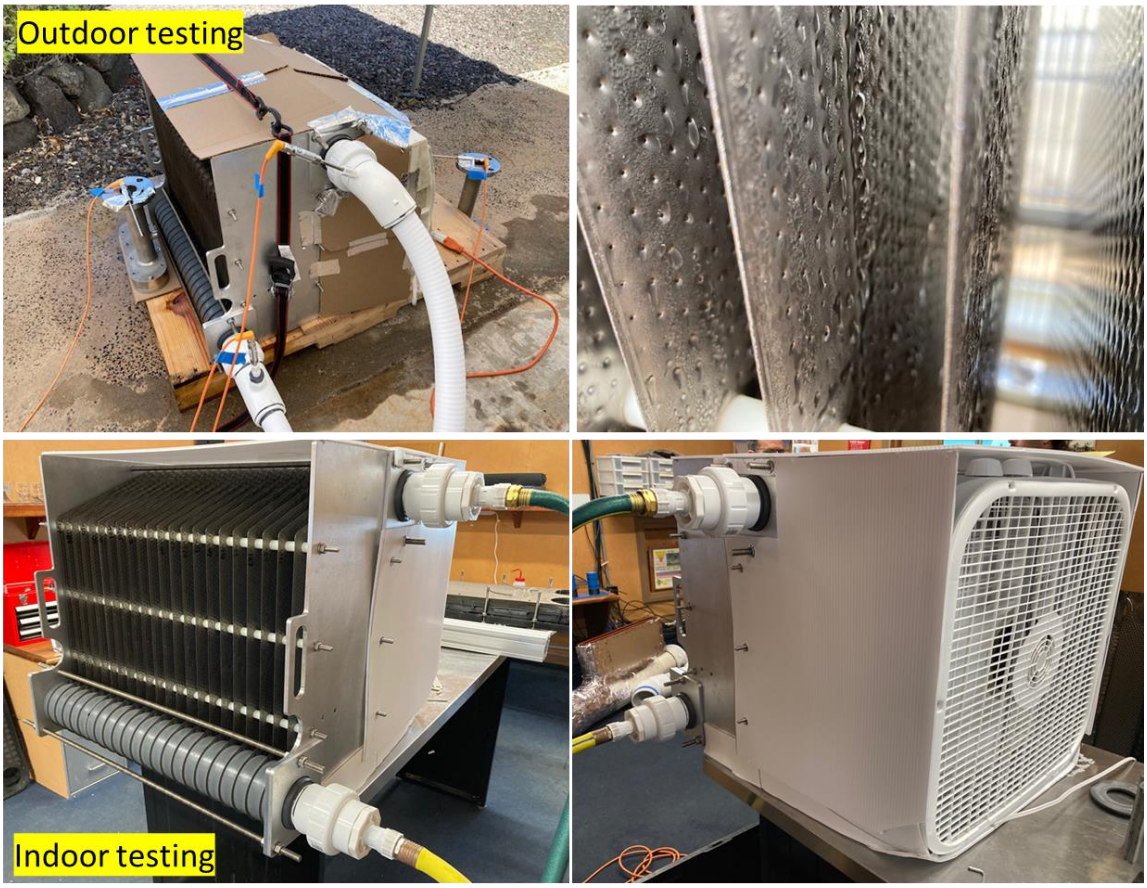

Figure 9. TFAC test setup.

For the outdoor testing, the unit was tested at four air flow rates (high, medium, low, off) and three cold seawater flow rates (5, 10, and 30 gpm) (Figure 10). Duty at no air flow is most likely due to a combination of wind effects (there was nothing to prevent air from flowing backwards over the plates), environmental heat input, and condensation (Figure 9, top right). As expected, highest cold seawater flow rate and high air flow rates provided the most duty.

For indoor testing, the same trends were observed but the duty was lower, possibly because the environmental heat input and humidity was lower and there was no wind effect.

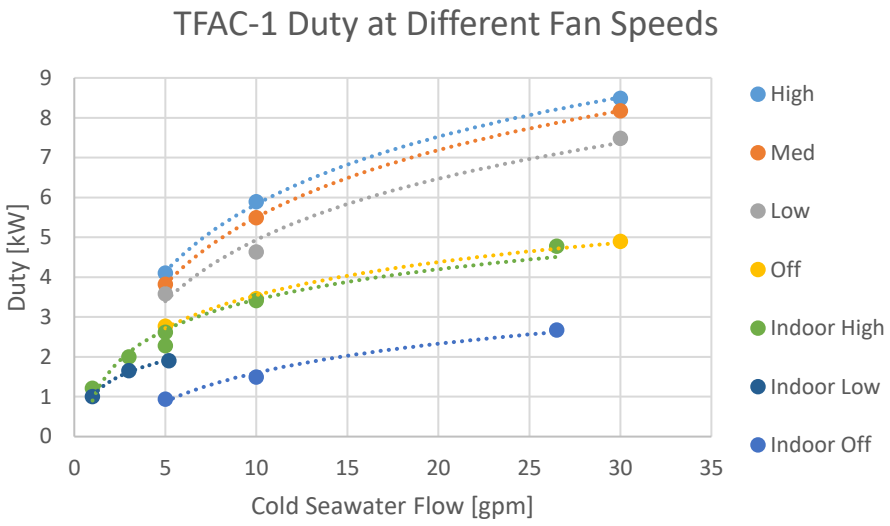

Figure 10. Duty vs seawater flow for different fan speeds.

Makai developed the TFAC because conventional window air conditioning units are not energy efficient *and* do not last long in a marine environment. The salt air is corrosive and shortens equipment lifespan. The TFAC's titanium plates are a perfect fit for this application. The box fan is considered a consumable unit and will require replacement, particularly if the unit is used outdoors.

Operational costs for the TFAC include cold seawater and electricity (for the fan) usage, which have to be balanced to provide sufficient cooling at a competitive (to existing AC units) operational cost.

4.2. WATER-WATER TFPX TESTING

Makai constructed one 6" TFPX unit for water-water testing in the 100 kW Test Station (Figure 11). The TFPX characteristics are summarized in Table 2.

Table 2. Overview of TFPX unit.

	# Plates	Plate Spacing [mm]	Foil Thickness ["]	Internal Channel Size [mm]	External Channel Size [mm]	Fluid Length [m]	HX Area [m2]
TFPX-1	50	2.01	0.004	0.44	1.366	0.39	5.475

The TFPX was tested with external flow rates from 7-300 gpm and internal flow rates from 5 to 36 gpm.

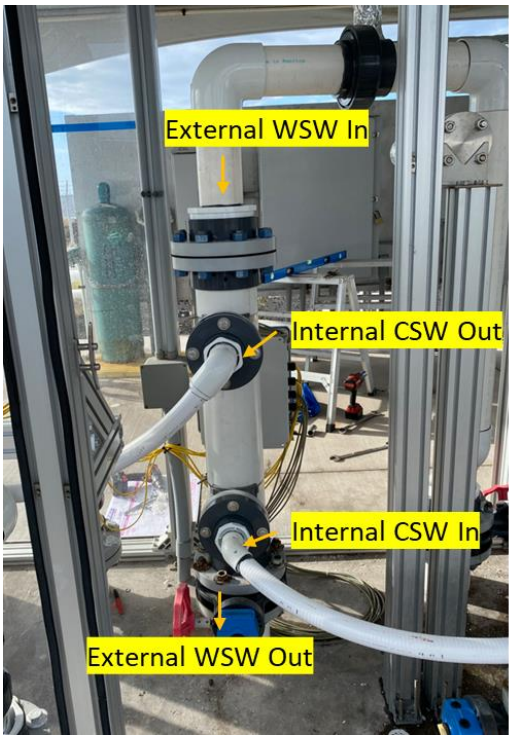

Figure 11. TFPX installed in the 100 kW Test Station.

Seawater pressure drops for the internal and external flows match with previously tested mid-length heat exchangers of comparable channel size (Figure 12 and Figure 13). In TFPX, the plates have varying widths corresponding to the cross section of the pipe. The actual internal flow through each plate is likely uneven and the actual flow velocity may be lower. The internal dP is reasonably in agreement with previous data from mid-length plates (INT3 and INT4).

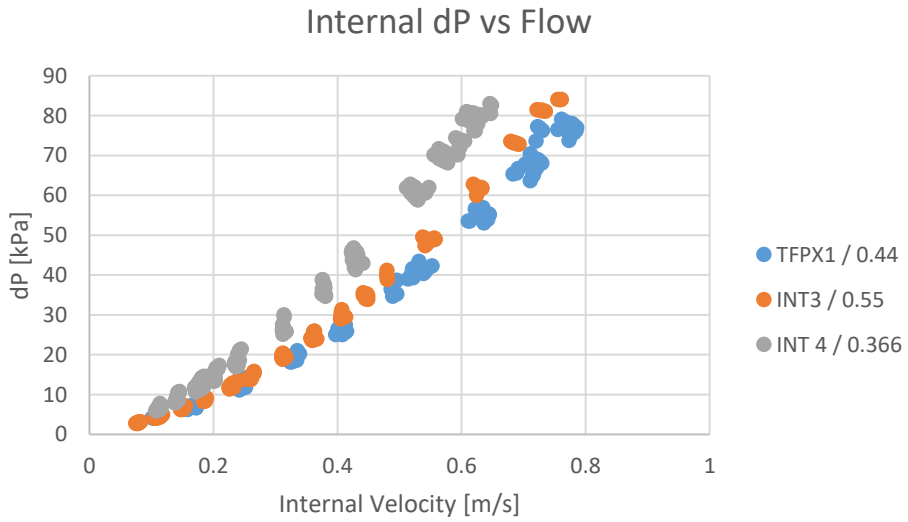

Figure 12. Internal dP vs velocity. The internal channel sizes of the INT units were slightly different than TFPX1.

The external dP vs flow is also agreement with INT3 which had the same channel size. A lower pressure drop was expected for the TFPX external flow because the external flow path is straight through; in the previous INT units, the external fluid path contained a 90 degree turn before entering the plates/channel and a 90 degree turn to the exit manifold. Makai expected these turns to add additional pressure drop. One potential explanation is in the TFPX, the external flow path is straight, but the path is constrained by the internal manifold at the entrance and exit. It is possible the manifold diameter in relation to the pipe diameter created a flow disturbance that resulted in a higher than expected pressure drop.

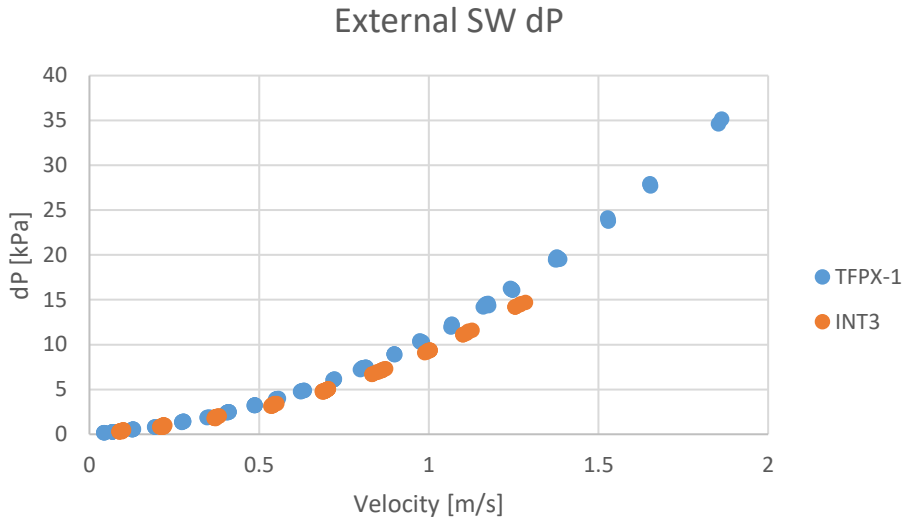

Figure 13. External dP vs velocity, INT3 and TFPX1 have external channel sizes = 1.36mm.

The overall heat transfer coefficient is dependent on both internal and external flow rates, as observed in previous water-water testing. TFPX1 internal and external convective coefficients are comparable to INT3 and INT4.

Overall, the 6" TFPX1 performance was comparable to previously tested mid-length INT units. The main advantage of the TFPX is the convenient form factor and the ability to remove and reinstall the plates without unstacking. In discussions with end users, ease of operation and maintenance, in addition to performance and cost, are key considerations in heat exchanger selection.

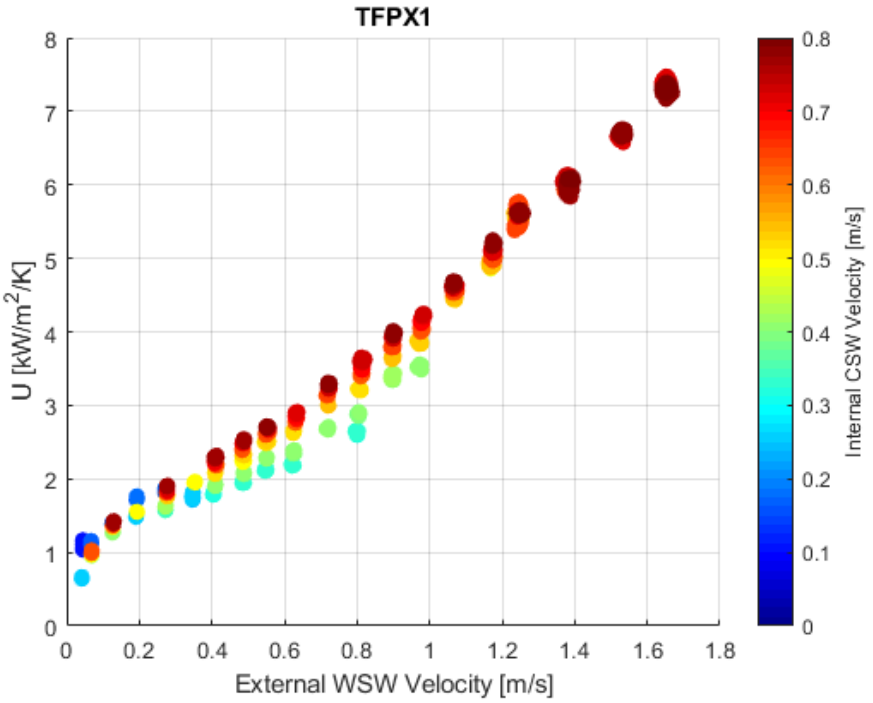

Figure 14. TFPX-1 overall heat transfer coefficient.

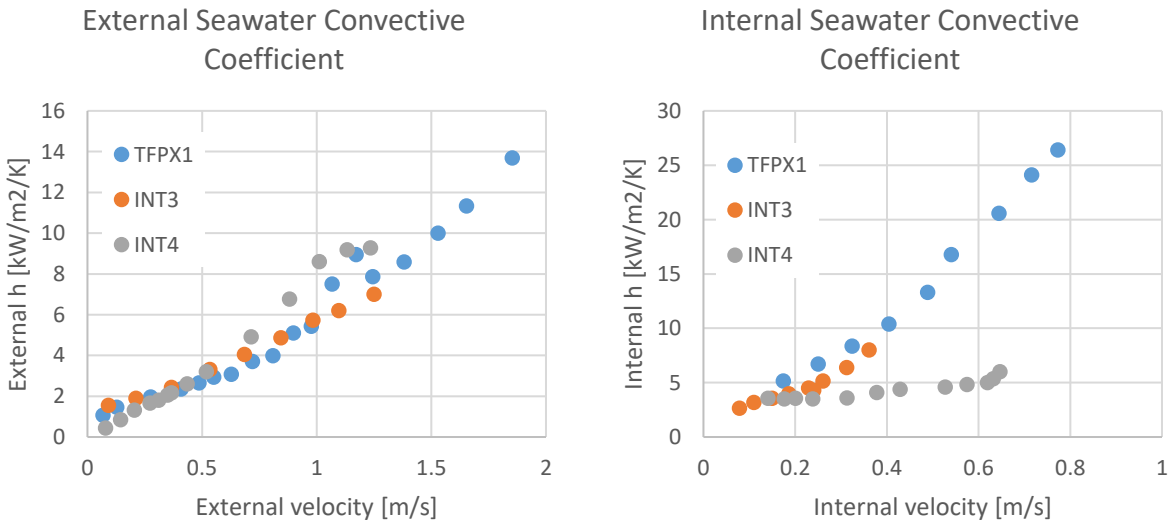

Figure 15. TFPX internal and external convective coefficients.

4.3. SEAWATER-AMMONIA TESTING

In this period, Makai built 7 stand-alone TFHX units with different internal/external channels and plate spacings (Table 3). Each unit was tested in a counterflow configuration as a condenser and an evaporator (except for TFHX-FL-8 which was tested as an evaporator only, Figure 16).

Table 3. Overview of TFHX test units.

	# Plates	Plate Spacing [mm]	Foil Thickness ["]	Internal Channel Size [mm]	External Channel Size [mm]	Fluid Length [m]	HX Area [m2]
TFHX-FL4	24	2.12	0.005	0.780	1.084	0.86	10.32
TFHX-FL5	12	2.12	0.005	0.780	1.084	0.86	5.16
TFHX-FL6	6	4.24	0.005	0.780	3.202	0.86	2.58
TFHX-FL7	12	2.12	0.005	0.503*	1.362*	0.86	5.16
TFHX-FL8	6	4.24	0.005	0.562	3.421	0.86	2.58
TFHX-FL9	12	2.12	0.005	0.560*	1.304*	0.86	5.16
TFHX-FL10	12	2.12	0.005	0.838	1.026	0.86	5.16

*Averaged channel sizes. Actual channel sizes varied across the plate.

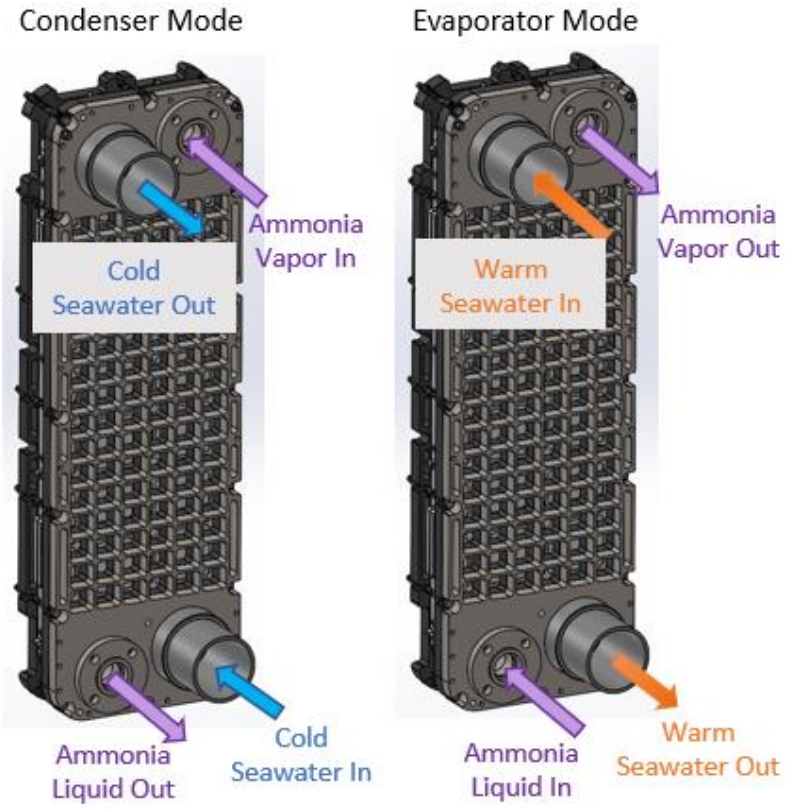

Figure 16. Full-length TFHX module configured for counterflow condenser and evaporator testing.

TFHX-FL-7 and FL-9 were designed with different patterns in the heat transfer area to test whether ammonia convection could be improved.

Except for FL-4, all the heat exchangers tested in this period consisted of 6 or 12 plates. The 12-plate heat exchangers have the same plate spacing as a full, 24-plate heat exchanger but use a flow blocker to take up half the volume in the module. Previous 24-plate tests were limited by the capacity of the 100-kW system. There was insufficient seawater flow to reach velocities > 1.5 m/s. Ammonia capacity was also limited to around 100 kW and because a 24-plate heat exchanger has 10.32 m^2 of heat transfer area, it was difficult to test at energy densities > 10 kW/m^2. A 12-plate test allowed testing at seawater velocities up to 2 m/s depending on the heat exchanger design and at power densities up to 22.5 kW/m^2. Furthermore, to investigate the effect of increasing seawater channel size, internal and external spacers were designed to double the plate spacing (i.e., increase the plate spacing from 2.12 mm to 4.24 mm). In this manner, two heat exchangers can have the same internal channel size but different external channel sizes.

Evidence of ammonia leaks were observed upon disassembly of multiple tests. Most of the leaks were attributed to issues with o-rings; either a pinched o-ring, misaligned o-ring, or deformations in the o-ring groove that led to imperfect sealing surfaces. Maintaining precise positioning of the o-rings is a known challenge; when plates are stacked and installed in a module, the module was not designed to provide full o-ring compression. Makai observed that mishandling the module during transport or installation into the 100 kW Test Station can lead to o-rings shifting out of place. Two leaks were suspected to be weld-related: a pinhole leak and a transition weld leak; neither leak was apparent during post fabrication pressure checks or during the overnight pressure check once a unit is stacked. Makai has learned more about fabrication and assembly requirements with each o-ring related leak and has also been exploring design options such as encapsulated o-rings to minimize future o-ring related leaks. Overall, any ammonia leakage was undetectable during environmental sampling or by abnormalities in seawater outlet temperature and the observed small leaks are not expected to affect performance testing results.

In condenser and evaporator configurations, each heat exchanger was tested at energy densities between 5-20 kW/m^2 and seawater velocities between 0.3-1.8 m/s. Ammonia duty was controlled by controlling the seawater flow rate through the companion (APV) heat exchanger. For example, during evaporator testing, the APV heat exchanger functions as a condenser; increasing the cold seawater flow through the APV increases TFHX duty at a fixed TFHX seawater flow rate. Seawater flow was controlled by adjusting seawater control valves. During evaporator testing, the quality is set by adjusting the ammonia liquid flow rate using a VFD to control the feed pump.

4.3.1. Seawater Pressure Drop

Seawater-side pressure drop is related to the pumping power required to provide a certain seawater flow rate through the heat exchanger. The seawater pressure drop is mainly dependent on channel size and velocity (Figure 17). At the same velocity, the pressure drop when tested as an evaporator versus a condenser should be comparable. Some plate designs exhibit limited expansion/contraction of the internal channel size with differences in internal vs external pressure and small deviations in pressure drop between evaporator and condenser mode are expected. However, substantial differences in pressure drop between evaporator and condenser modes (for the same velocity) were observed in FL7 (Figure 18).

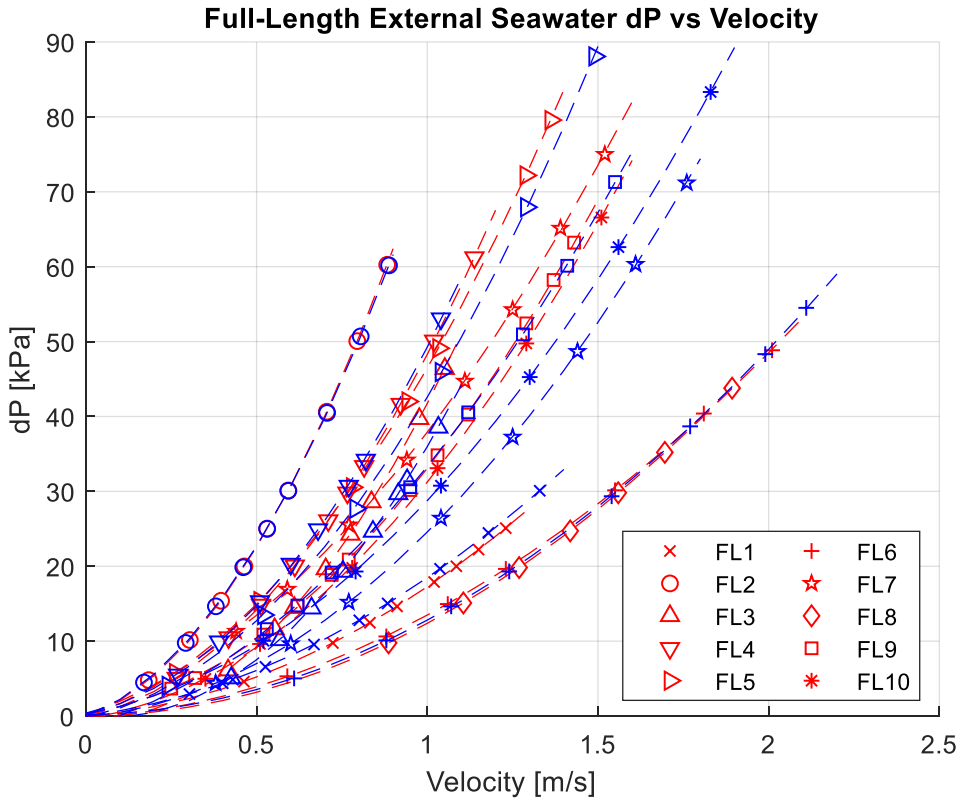

Figure 17. Seawater pressure drop for all ten TFHX units. Evaporator data is in red and condenser data is in blue.

This discrepancy was caused by a small ammonia leak into the area between the internal and external seal welds which inflated foil and blocked off some of the flow area between the manifold and the channel. Heat exchangers are usually tested as a condenser first and the maximum ammonia pressures during condenser testing are typically lower than that of evaporator testing, it is likely the leak developed during evaporator testing or maximum inflation occurred during evaporator testing, leading to higher seawater pressure drops observed during evaporator testing compared to condenser testing.

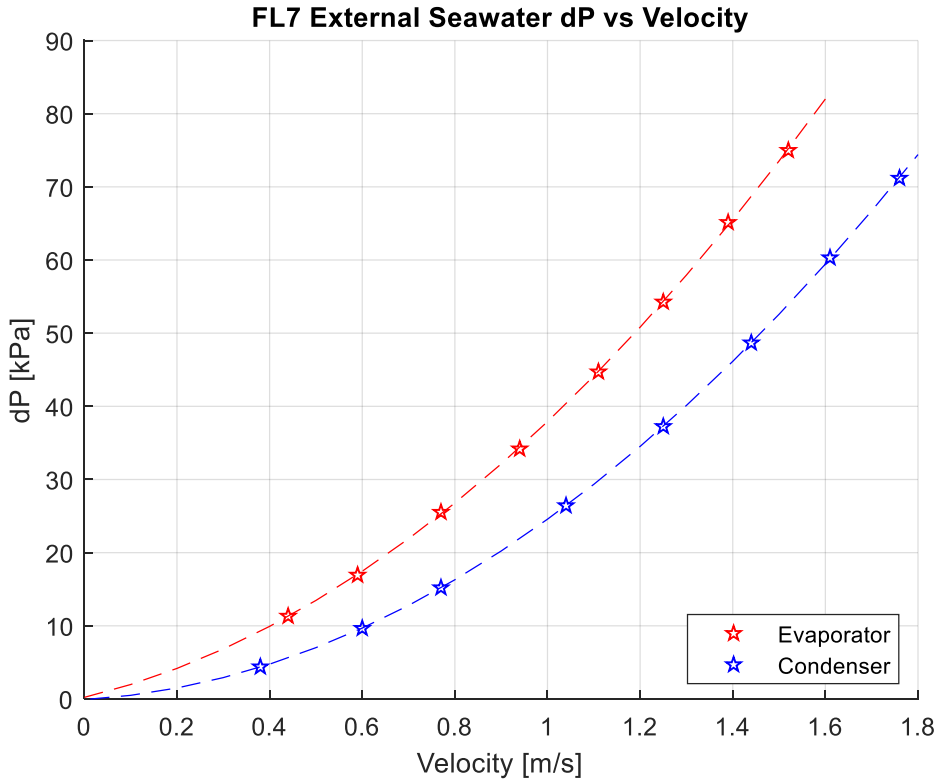

Figure 18. Substantial discrepancy in seawater pressure drop between condenser and evaporator tests.

4.3.2. Ammonia Pressure Drop

Ammonia-side pressure drop is an important consideration for an evaporator/condenser. In a closed-cycle OTEC system, minimizing the pressure drop increases the available differential pressure across a turbine and reduces the pumping power required to recirculate refrigerant. Ammonia pressure drop is strongly dependent on ammonia vapor flow rate, quality, and heat exchanger geometry.

As a condenser, among the FL units with uniform internal channel sizes, ammonia pressure drop was highest in the FL-1 which had the smallest internal channel (0.59 mm) and lowest in FL-2, FL-3, and FL-10 which had largest internal channels. A circle weld was used in FL-2 and FL-3 to produce a 0.90 mm effective internal channel size whereas a dot weld was used in FL-10 to produce a 0.84 mm effective internal channel. The aspect ratios and the actual geometry of the internal channel is different and may be why there is no significant difference in the ammonia pressure drop between the two designs. Both FL units with varying internal channels (FL-7 and FL-9) had the smallest averaged (overall) effective internal channel sizes and the highest pressure drops. It is possible the vapor portion of the plate design did not encompass the vapor sections of the unit (i.e., duty was distributed such that vapor was present in sections with the small internal channels).

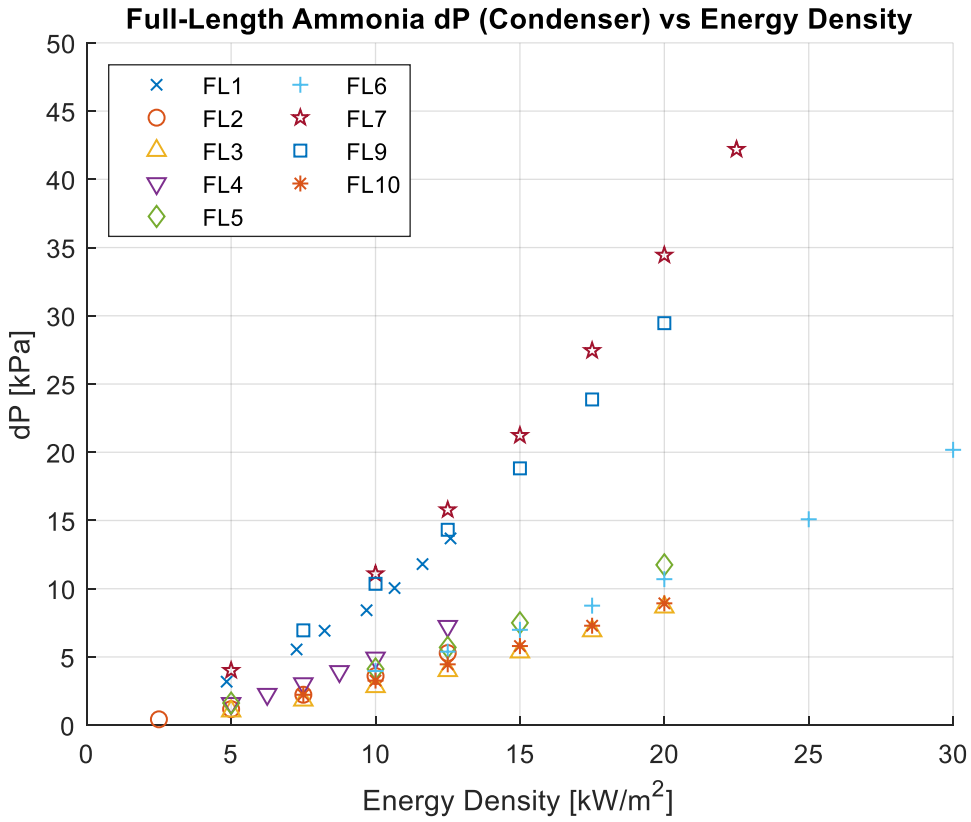

Figure 19. Ammonia pressure drop in condenser mode.

In evaporator mode, the same trends as condenser ammonia pressure drop were observed; of the plates with uniform internal channels, smaller channels had higher pressure drops and varying channel designs of FL-7 and FL-9 produced the highest pressure drops. FL-1 through FL-8 were tested at 60-70% quality and FL-9 and FL-10 were tested at 50% quality; in this range, quality variations did not have a significant impact on pressure drop.

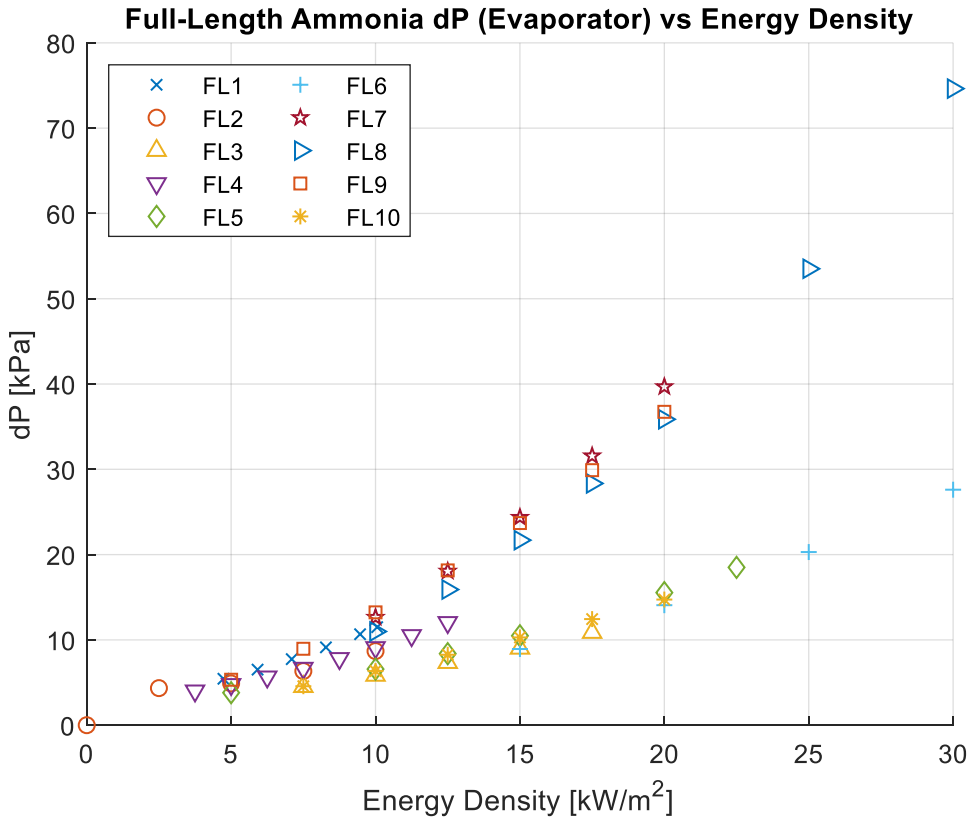

Figure 20. Ammonia pressure drop in evaporator mode.

4.3.3. Overall Heat Transfer Coefficient

U-value is predominantly dependent on seawater flow rate but duty (and quality for an evaporator) also have an effect. In this period, Makai changed the log-mean temperature difference (LMTD) calculation for the evaporator use the ammonia saturation temperature at the evaporator outlet pressure and re-calculated U-value using this new LMTD (see Section 8.2.3 and 8.2.5). In both condenser and evaporator modes, U-value increases logarithmically with increasing seawater flow (Figure 21 and Figure 22).

There is no clear trend in U-value versus energy density (Figure 23 and Figure 24). As an evaporator, U-values increase slightly (~10%) or remaind the same with increasing energy density. As a condenser, increases, decreases, and no changes in U value have been observed with increasing energy density. In FL-7 and FL-9 (designs with varying internal channel sizes), U-value appears to increase with increasing energy density in condenser mode but decrease with increasing energy in evaporator mode.

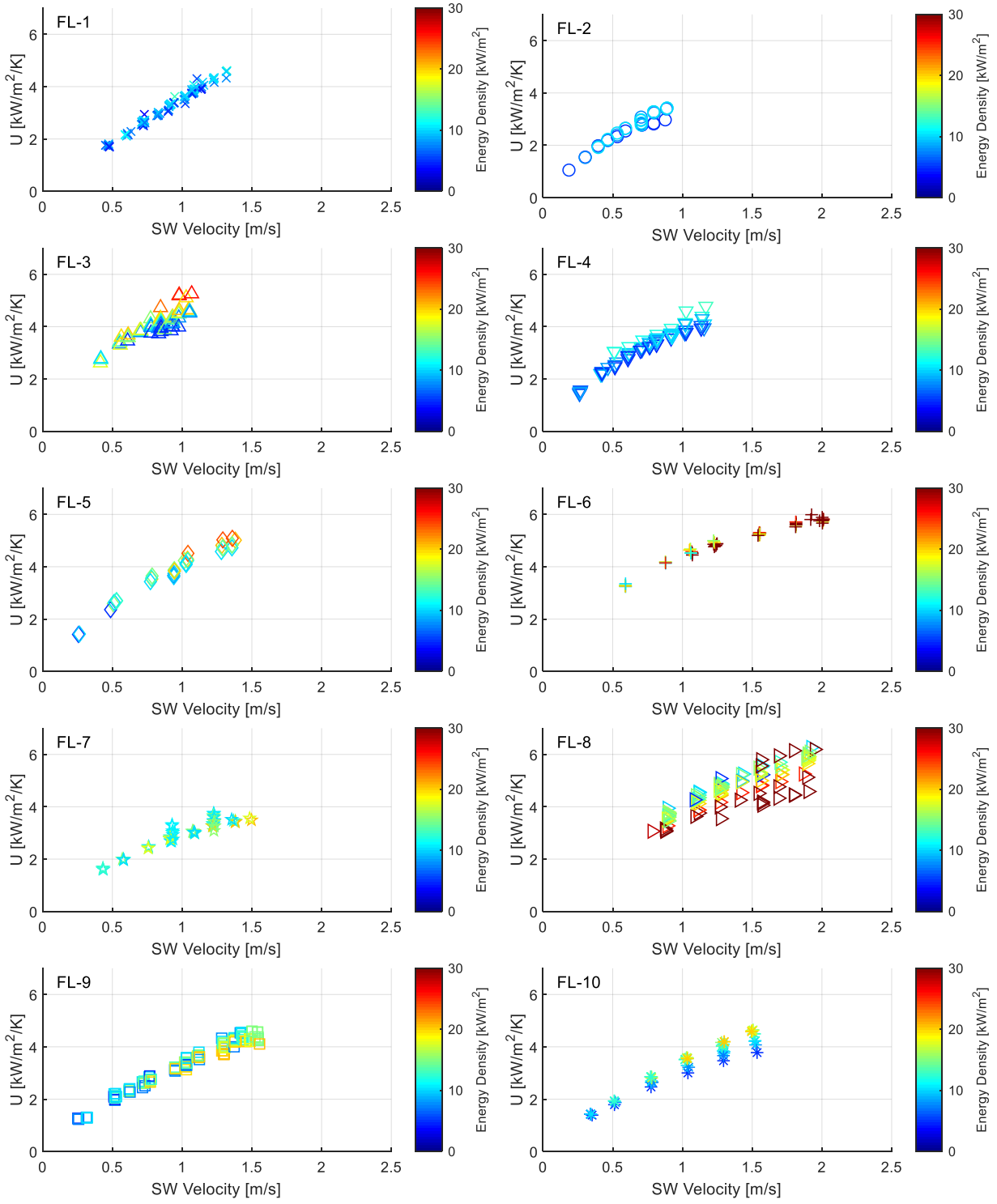

Figure 21. Evaporator U-value vs seawater velocity.

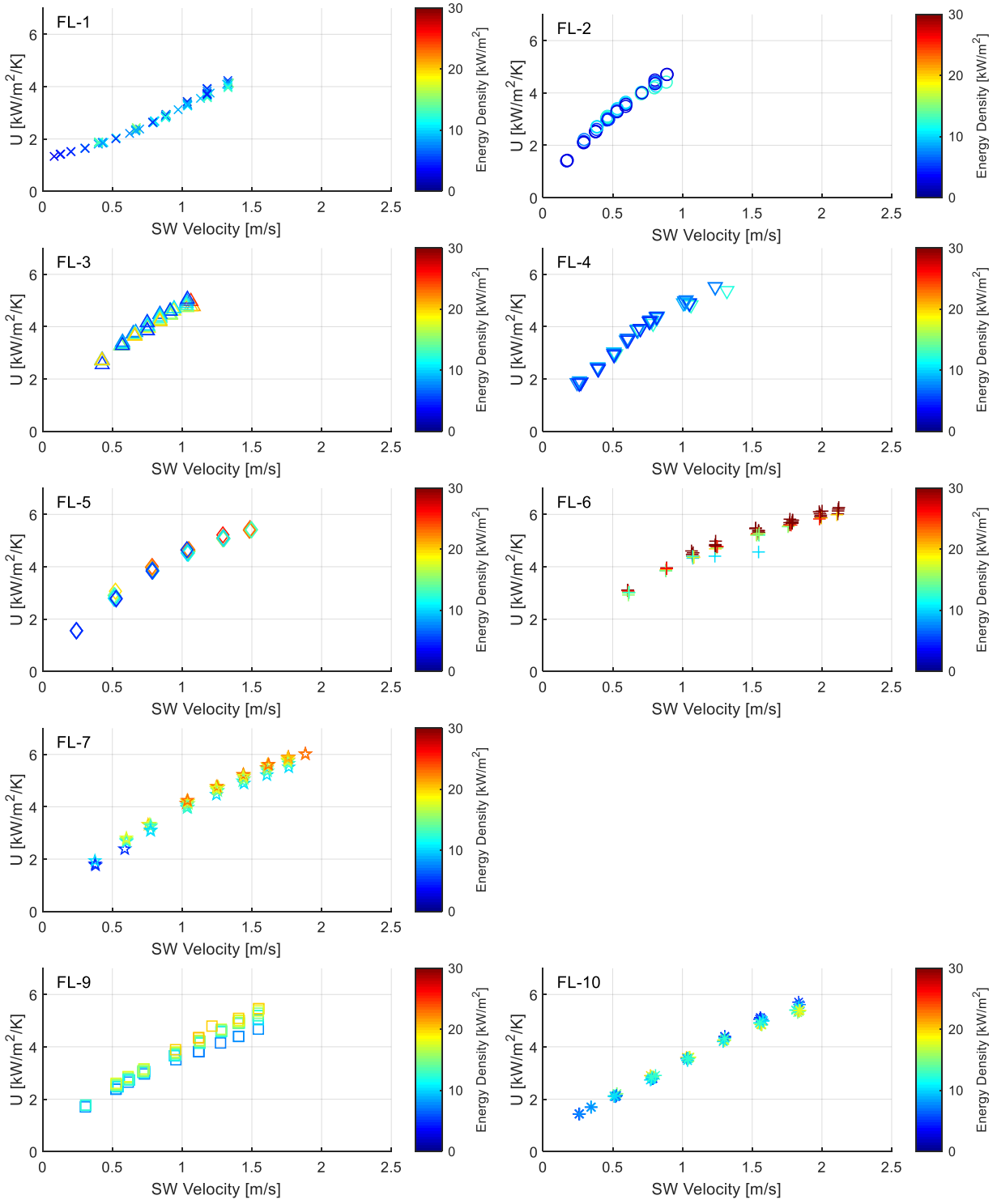

Figure 22. Condenser U-value vs seawater velocity.

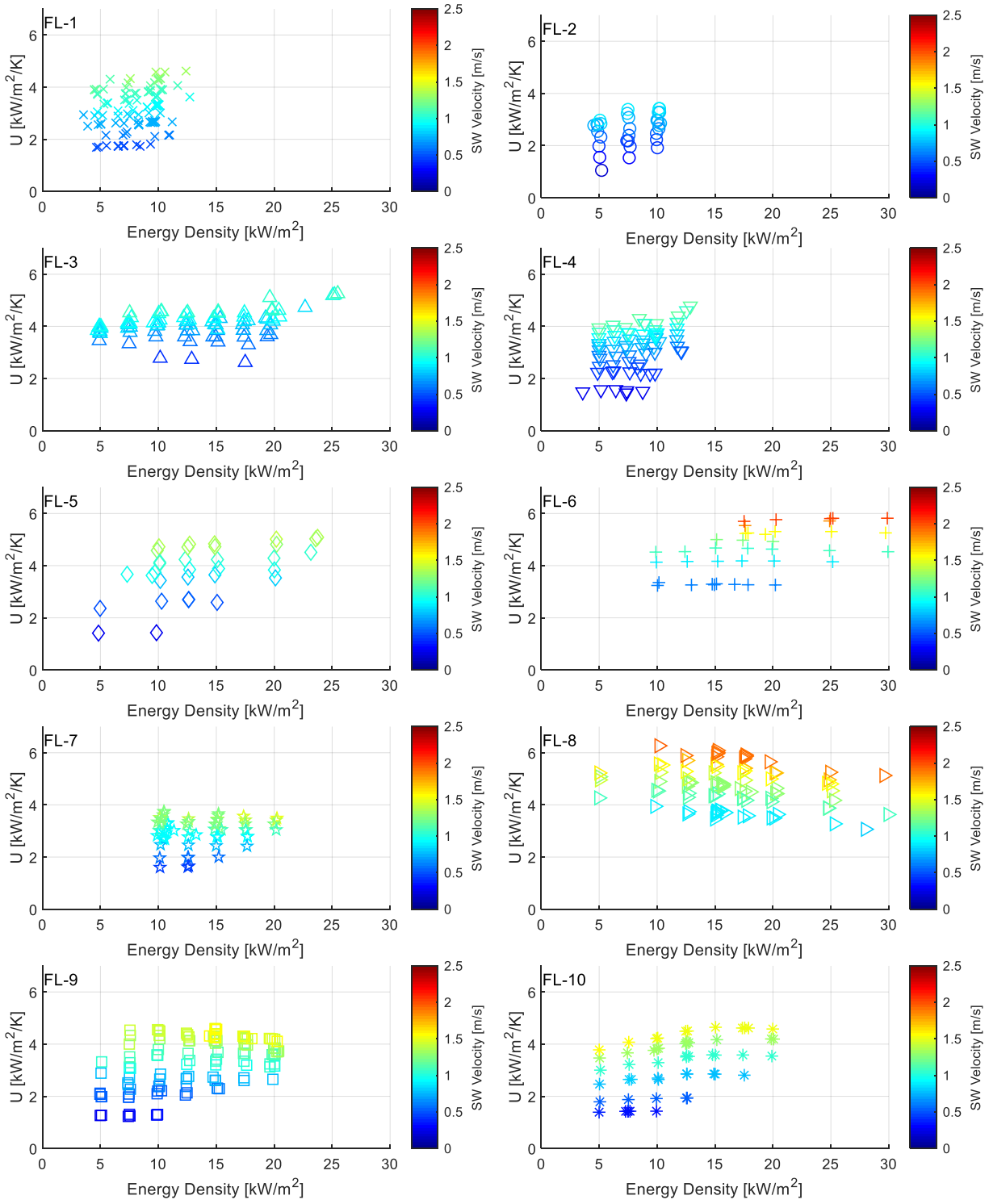

Figure 23. Evaporator U-value vs energy density.

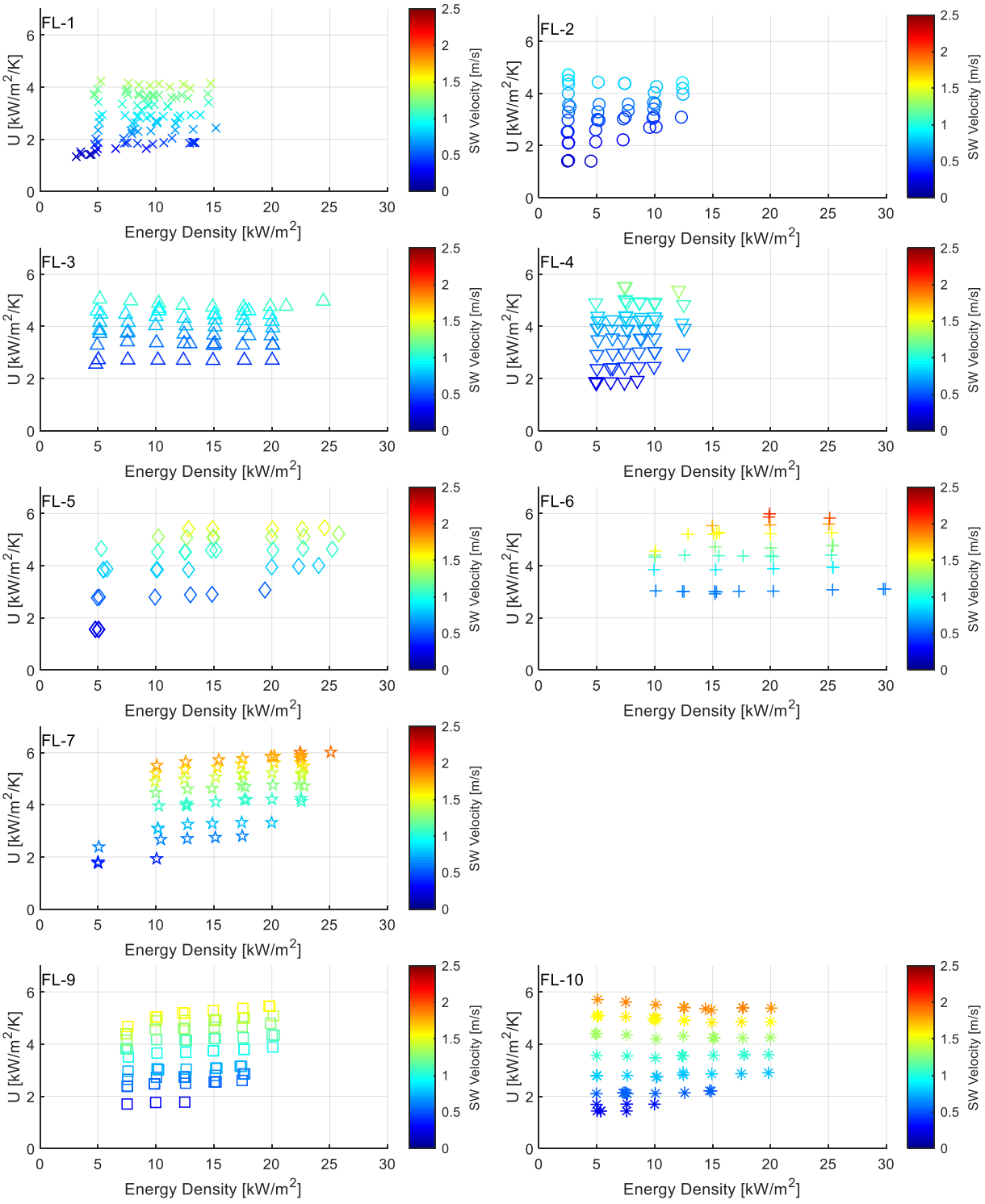

Figure 24. Condenser U-value vs energy density.

4.3.4. Convective Coefficients

Ammonia and seawater convective coefficients were calculated for each TFHX using a constrained least-squares solver, where the lower bound for the convective coefficients is 0 (Section 8.2.6).

Makai has previously reported convective coefficients but now believes there is substantial uncertainty surrounding the convective coefficients. When used for the same heat exchanger, the ammonia and seawater convective coefficients can be used to predict overall heat transfer coefficients at untested operating points. When solving for convective coefficients, there are more unknowns than equations and, therefore, there are multiple solutions. The least-squares solver provides a solution which minimizes the overall error but any measurement uncertainties will skew the results.

Apart from the mathematical uncertainties, the physical reasoning behind Makai's shift away from comparisons based solely on the convective coefficients is that the overall heat transfer coefficient is averaged across the entire plate, which assumes heat transfer is evenly distributed across the entire plate. This assumption is likely flawed, particularly for FL-7 and FL-9 which had different patterns throughout the heat transfer area. The overall heat transfer coefficient is still reflective of the unit's performance (as a whole) but using the convective coefficients derived from the overall heat transfer coefficient as the primary method to compare different heat exchange designs can be misleading and is no longer recommended. The most reliable comparisons are made using direct measurements and values calculated directly from measurements, i.e., heat exchanger operating pressure or approach temperature. However, Makai will provide the convective coefficients in this report for continuity.

Seawater Convective Coefficients

Seawater side convective coefficients were solved independently for each configuration (condenser or evaporator) for each TFHX unit. Except for FL-10, the external seawater convective coefficients are in agreement (Figure 25). As in previous results, seawater convective coefficients increase almost linearly with increasing seawater velocity.

There is no clear trend in convective coefficient versus the channel size (Figure 26). Heat exchangers with large seawater channels (FL-3 and FL-6) had among the highest seawater convective coefficients for the same velocity, but FL-8, which also had large seawater channels had lower seawater convective coefficients compared to heat exchangers with smaller seawater channels such as FL-5.

Ammonia side convective coefficients.

Ammonia-side convective coefficients also did not have a clear trend with ammonia channel size (Figure 27). Makai suspects smaller internal channels may have higher convective coefficients due to vapor shear. However, when designing for an application, improvements in effectiveness must also be balanced by penalties associated with higher pressure drops.

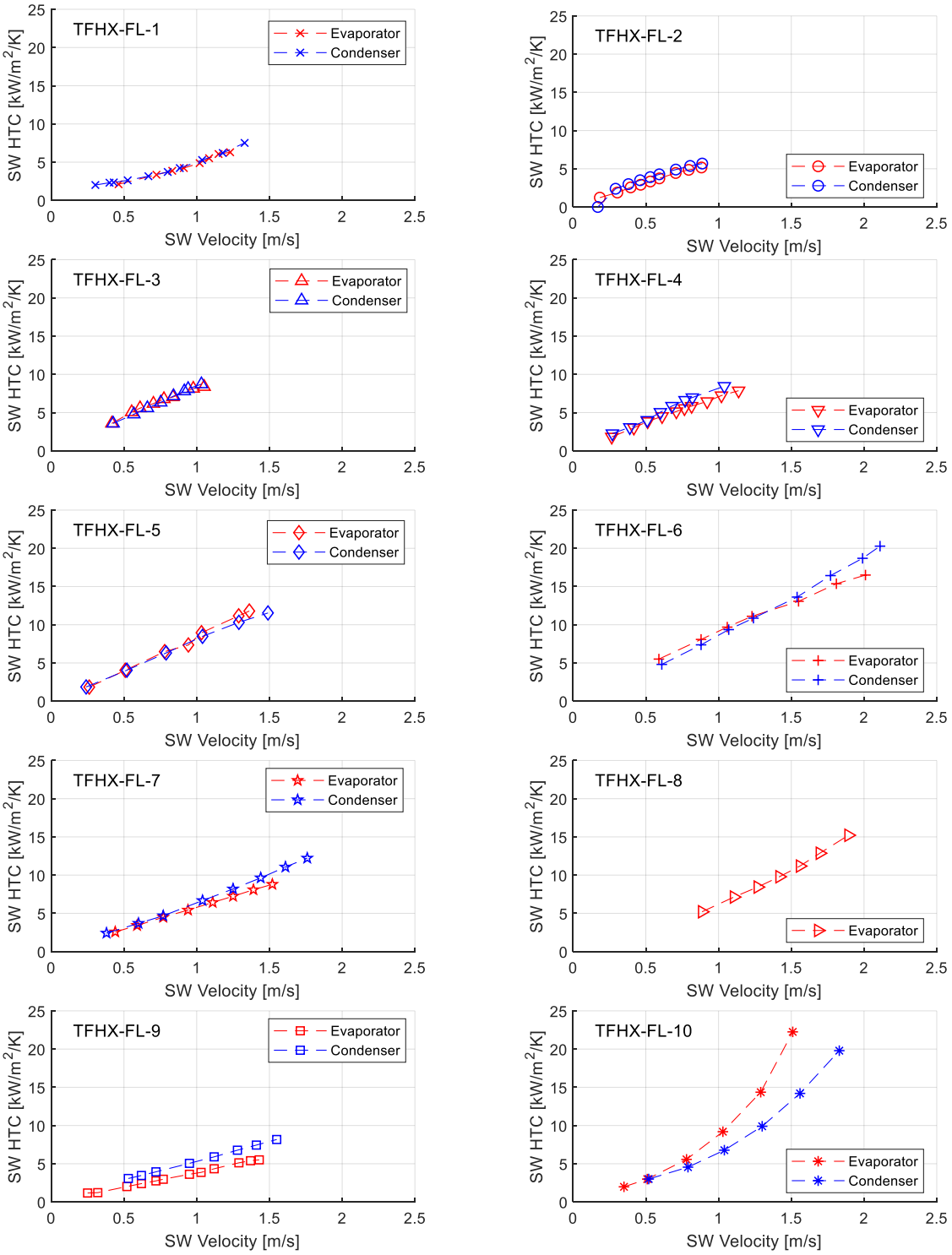

Figure 25. Seawater-side convective coefficients calculated individually for each configuration showed strong agreement.

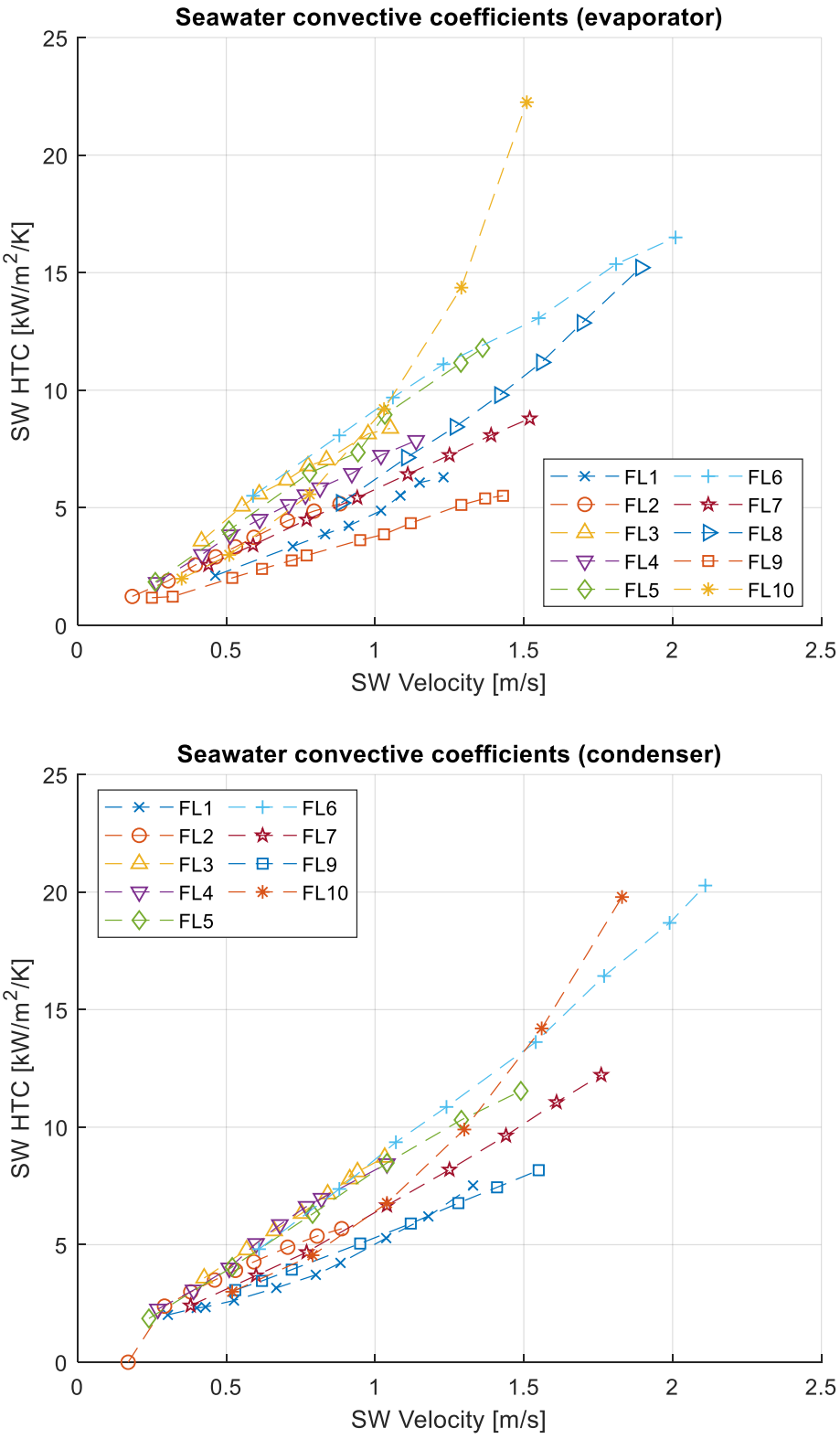

Figure 26. External seawater convective coefficients for all ten TFHX designs.

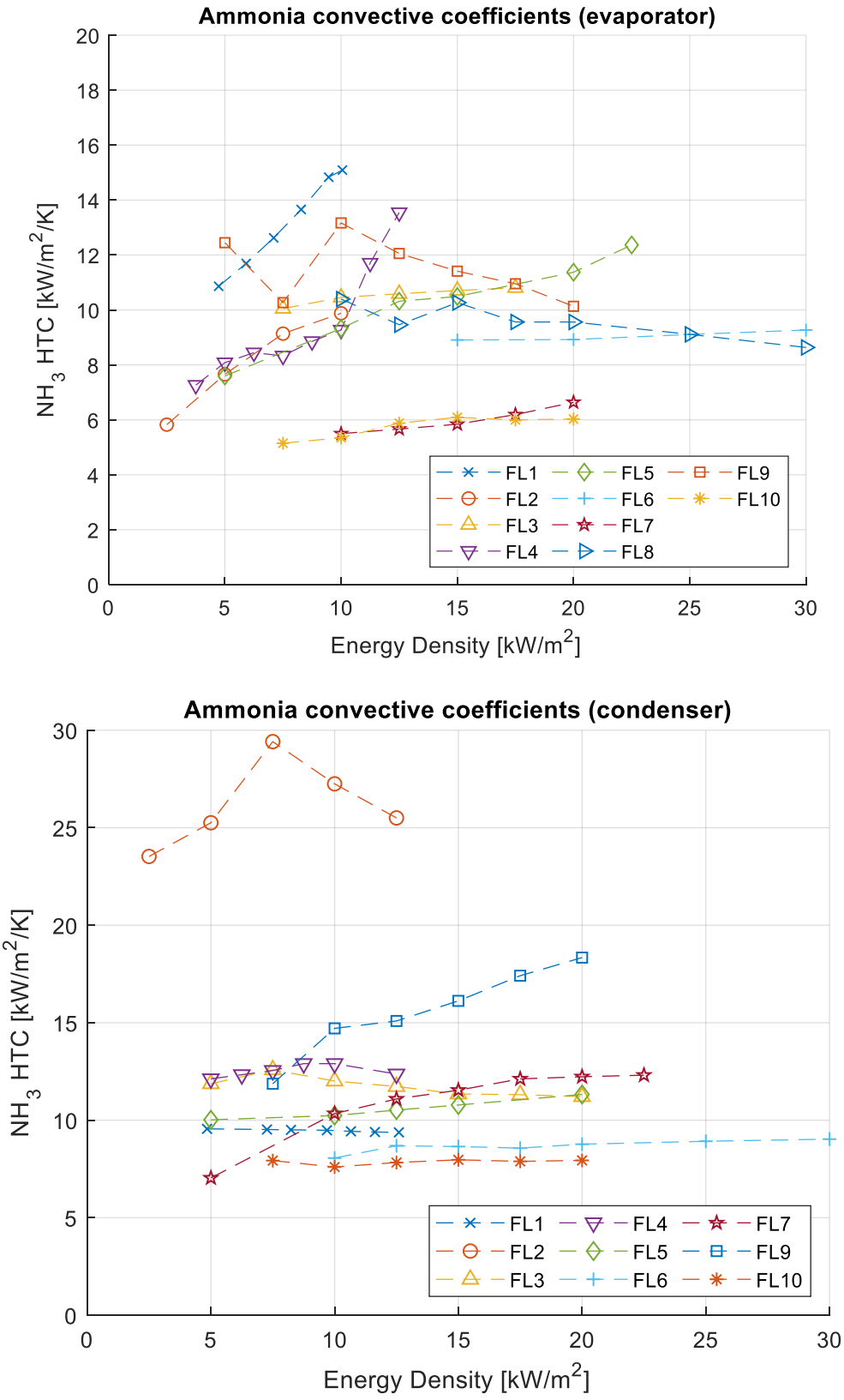

Figure 27. Ammonia-side convective coefficients for condenser and evaporator.

4.3.5. Heat Exchanger Approach Temperature

Heat exchanger approach temperature is determined by the seawater temperature, seawater flow rate, and duty. Makai is defining the approach temperature as:

$$T_{approach} = T_{warm\ seawater\ in} - T_{saturation\ at\ EOPS} \text{ (evaporator)}$$

$$T_{approach} = T_{saturation\ at\ CIPS} - T_{cold\ seawater\ in} \text{ (condenser)}$$

Makai's definition is customized for OTEC purposes; the ammonia saturation temperatures at the evaporator outlet and condenser inlet are used because these are directly connected to the turbine inlet/outlet. Additionally, because the bulk of the duty is in phase change, superheating at the condenser inlet is not accounted for and the saturation temperature is used instead of the measured temperature.

For OTEC operations, small approach temperatures result in higher available differential pressure across the turbine. Higher seawater flow rates yield smaller approach temperatures, but also require higher parasitic losses from high volumetric flow rates and/or high seawater pressure drops.

One way to compare heat exchanger performance is to match heat transfer areas and then compare the approach temperature versus pumping power at fixed energy densities (Figure 28 and Figure 29).

For both evaporator and condenser modes, TFHX units with 4.24-mm plate spacings (FL-3, FL-6, and FL-8) and, therefore, larger seawater channels, had the lowest approach temperatures for the same pumping power. FL-1 had the lowest approach temperature of the TFHX units with 2.12-mm plate spacing and also had comparable approach temperatures compared to FL-3.

This analysis only considers the pumping power through the heat exchanger. For OTEC operations, the total volume of seawater flow is also important, particularly for the condenser. For example, although FL-3 and FL-6 had the lowest condenser approach temperatures, the both required up to 2.5X the flow as FL-4. Furthermore, at the same pumping power, FL-4 had 10% higher approach temperature than FL-1 but used 20% less volumetric flow. For a fixed cold water pipe size, lower volumetric flow rates have lower seawater system losses.

A comprehensive comparison of TFHX designs in the OTEC context will require a tradeoff study evaluating increase in net power production gained by smaller approach temperatures versus a larger cold water pipe and overall OTEC system (i.e., more expensive capital investment).

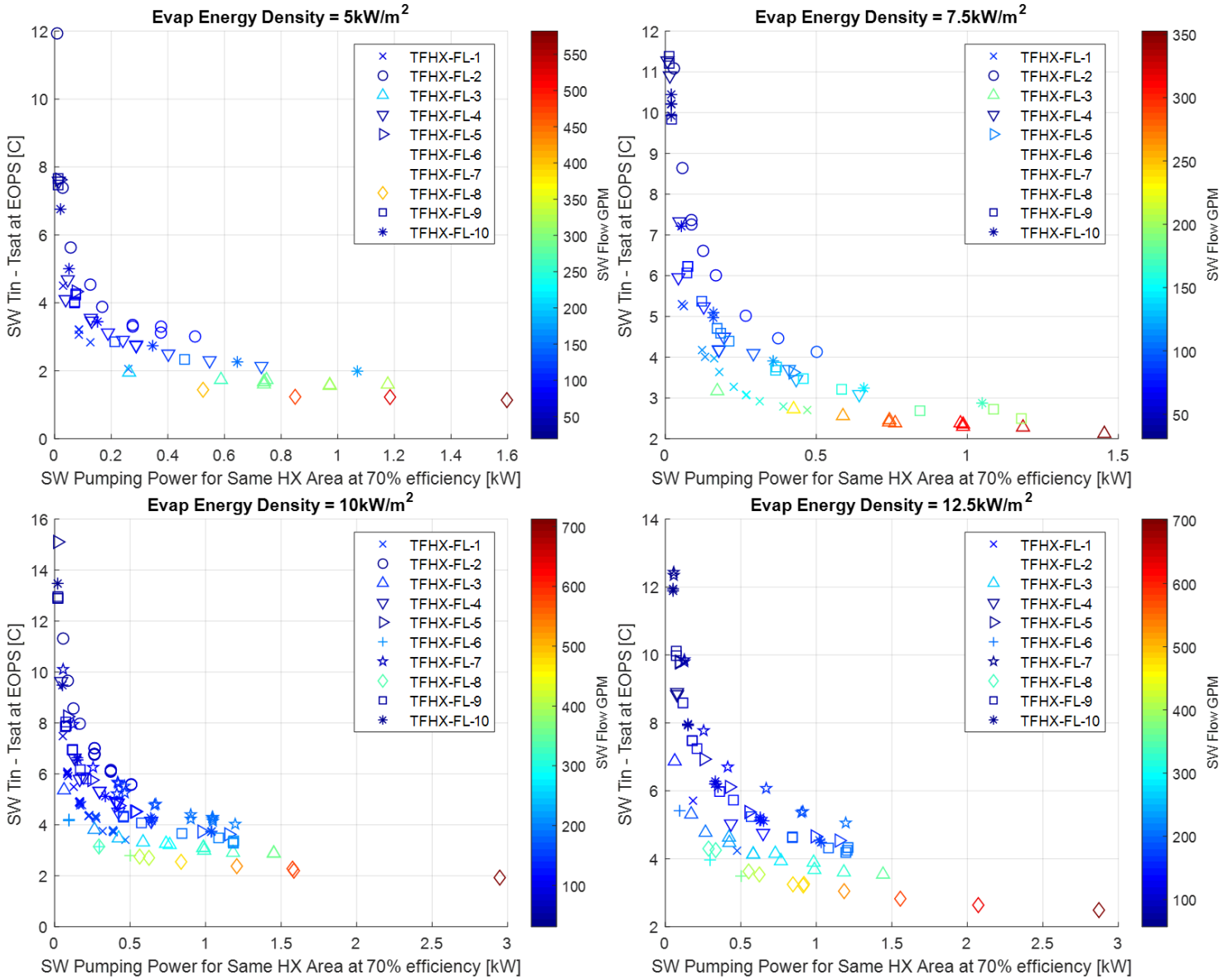
Evap Energy Density = 5kW/m2
Evap Energy Density = 7.5kW/m2
Evap Energy Density = 10kW/m2
Evap Energy Density = 12.5kW/m2
SW Tin - Tsat at EOPS [C]
SW Pumping Power for Same HX Area at 70% efficiency [kW]
SW Flow GPM
TFHX-FL-1
TFHX-FL-2
TFHX-FL-3
TFHX-FL-4
TFHX-FL-5
TFHX-FL-6
TFHX-FL-7
TFHX-FL-8
TFHX-FL-9
TFHX-FL-10

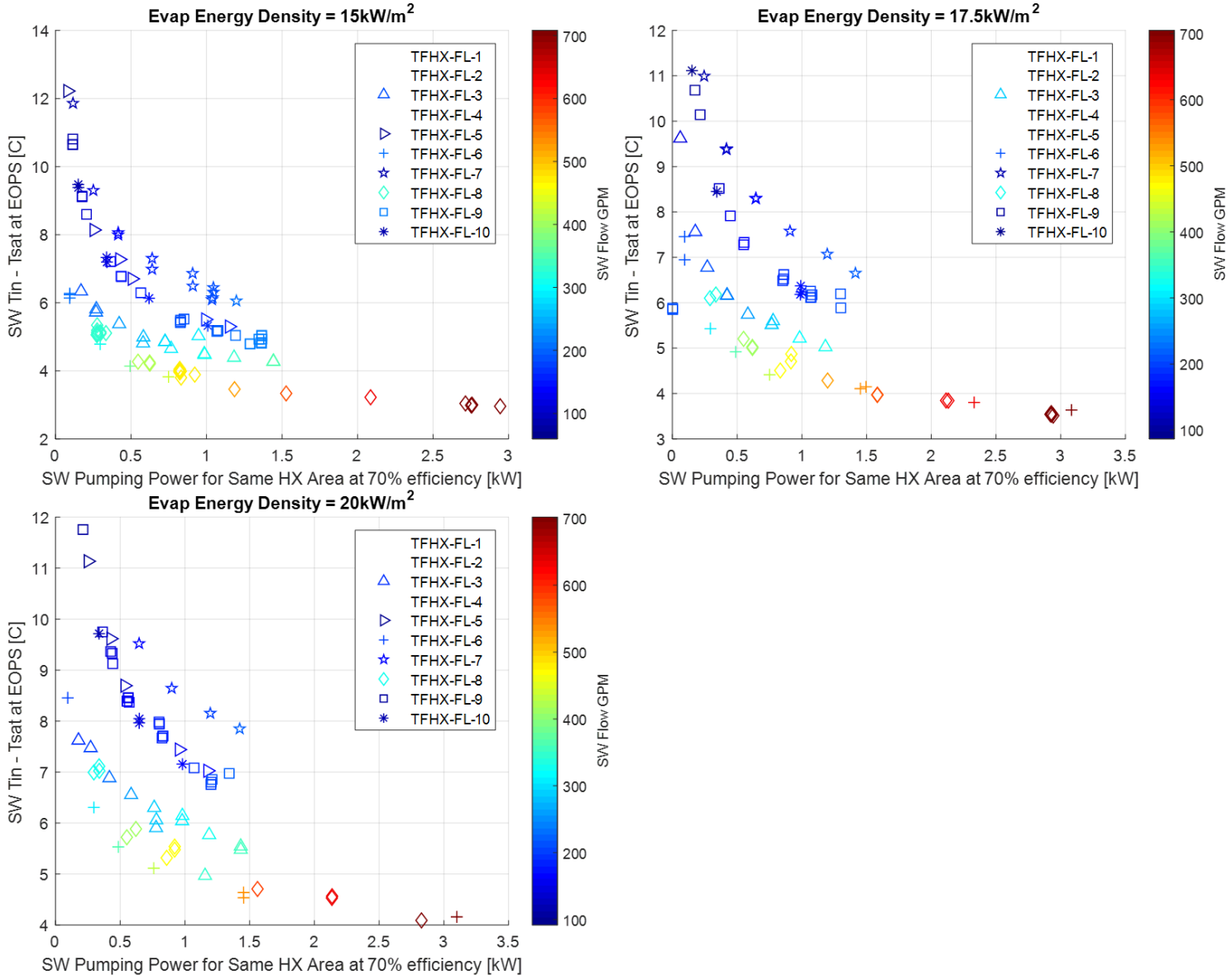

Figure 28. Evaporator approach temperature vs pumping power at different energy densities.

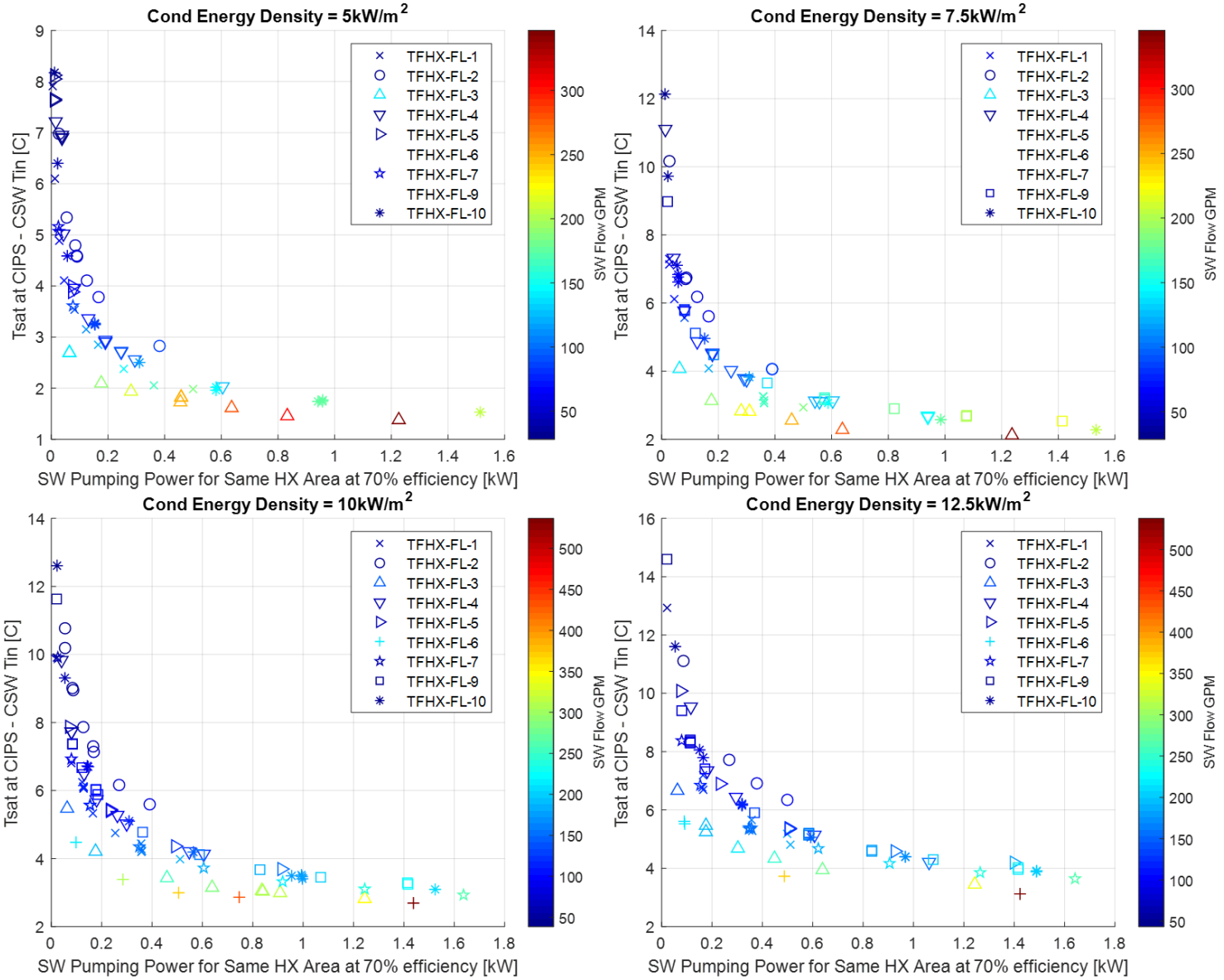
Cond Energy Density = 5kW/m 2
Cond Energy Density = 7.5kW/m 2
Cond Energy Density = 10kW/m 2
Cond Energy Density = 12.5kW/m 2
Tsat at CIPS - CSW Tin [C]
SW Pumping Power for Same HX Area at 70% efficiency [kW]
SW Flow GPM
TFHX-FL-1
TFHX-FL-2
TFHX-FL-3
TFHX-FL-4
TFHX-FL-5
TFHX-FL-6
TFHX-FL-7
TFHX-FL-9
TFHX-FL-10

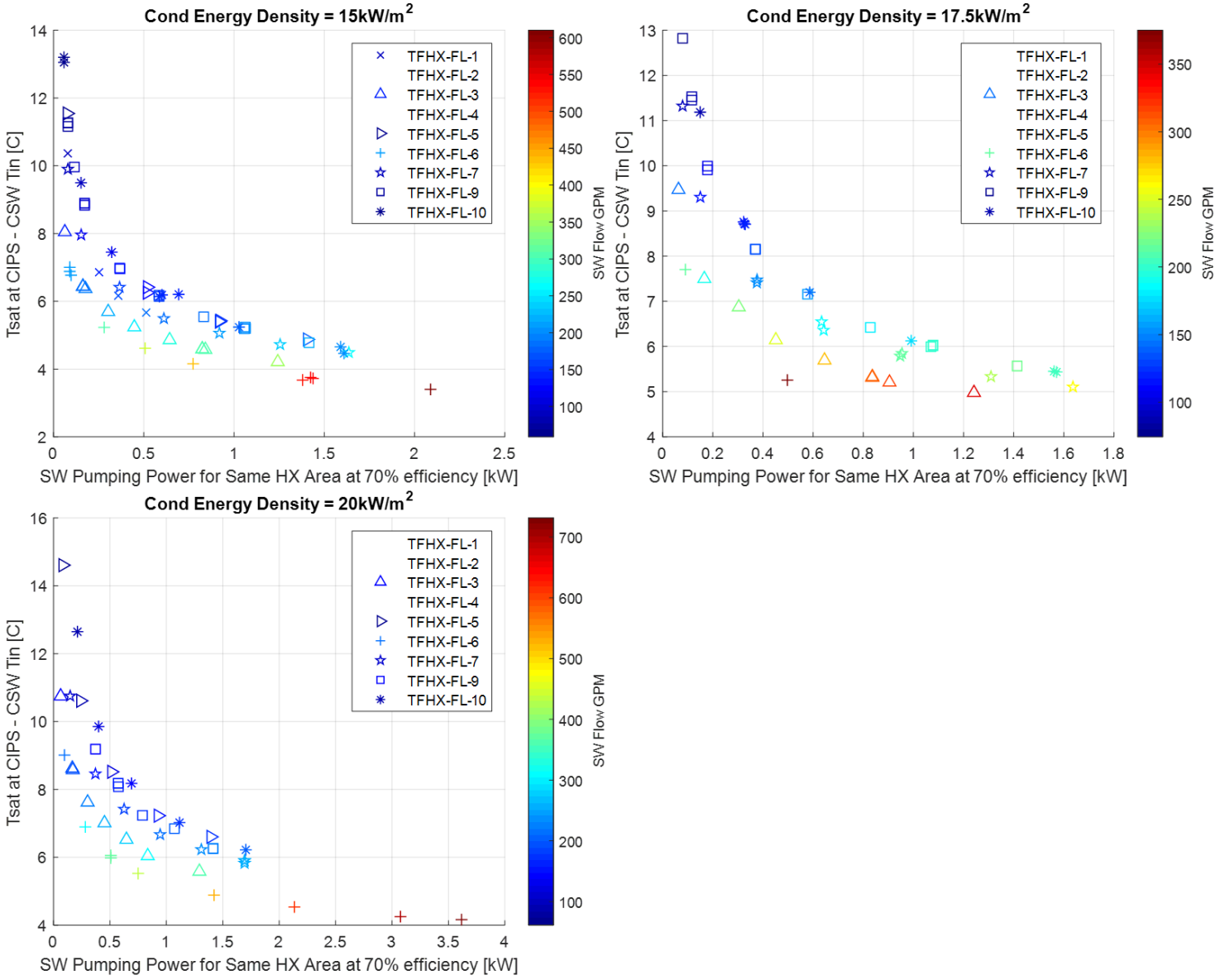

Figure 29. Condenser approach temperature vs pumping power at different energy densities.

4.4. DISCUSSION

4.4.1. Compactness

TFHXs contain more heat transfer area per cubic meter (m2/m3) than plate-and-frame, brazed fin, and shell-and-tube heat exchangers (Figure 30). FL-1 type (2.12-mm plate spacing units) and FL-3 type (4.24-mm plate spacing units) are in the same range of compactness compared to previous TFHX designs. At the same energy density, TFHXs require less than 25% of the volume of previously tested heat exchangers to produce the same duty (Figure 31).

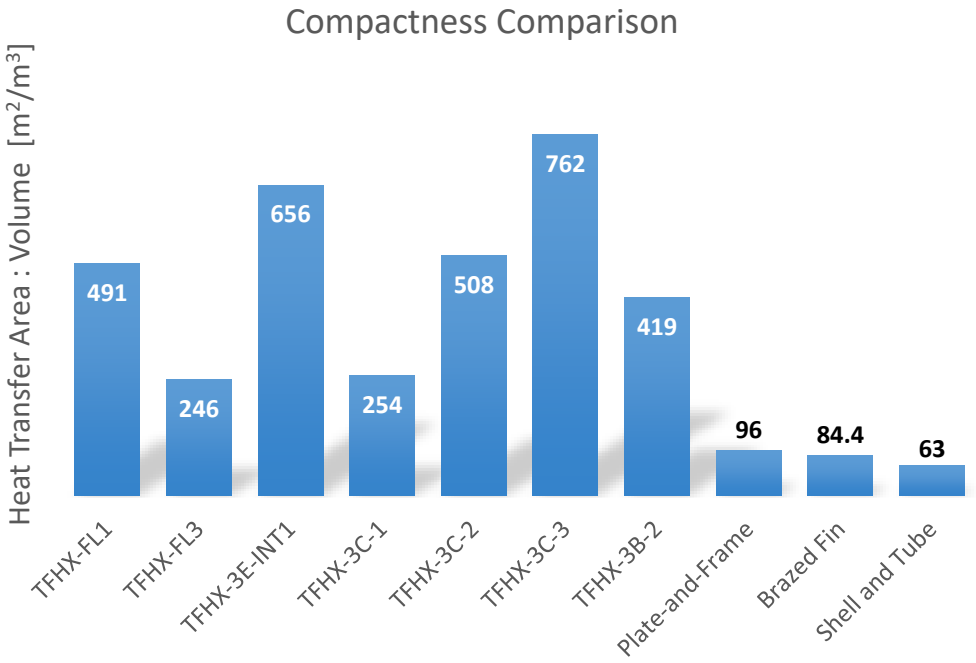

Figure 30. TFHX heat exchangers have more heat transfer area per volume compared to the previously tested plate-frame (APV), brazed fin (BAHX3), and shell and tube (ETHX) heat exchangers

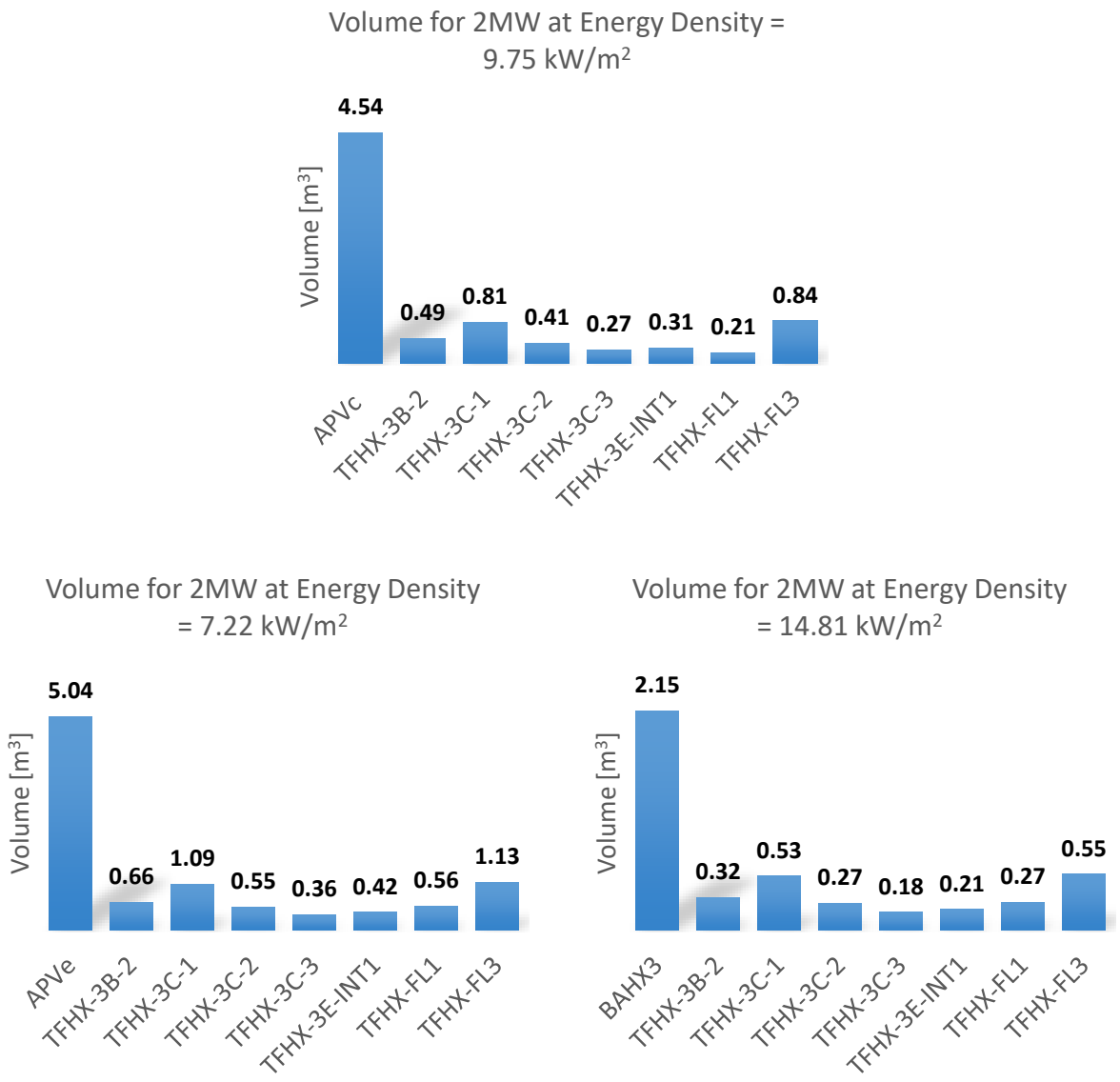

Figure 31. Comparison of volume required for 2MW of duty at various energy densities. Energy density was selected to match previously tested heat exchangers.

4.4.2. OTEC Heat Exchanger Design

Makai previously reported on the development of the OTEC Power Calculator, a tool to evaluate different heat exchanger designs in the context of an OTEC system performance. Heat exchangers can be compared in terms of area (i.e., heat exchanger cost) or volume (i.e., system size and cost) required to produce a targeted net power.

In this analysis, to provide comparison between heat exchanger designs, the OTEC system (i.e., cold water pipe size and turbine performance characteristics) is fixed. This assumption is intended to fix the cost of the OTEC system components. The annual average net power production, heat exchanger area, and heat exchanger volume are compared.

Starting with a FL-4 as a condenser using 12,000 gpm of cold seawater, different evaporator designs (FL-1 to FL-9) were scaled to the same area and evaluated by changing the warm seawater flow to maximize the average annual net power (Figure 32).

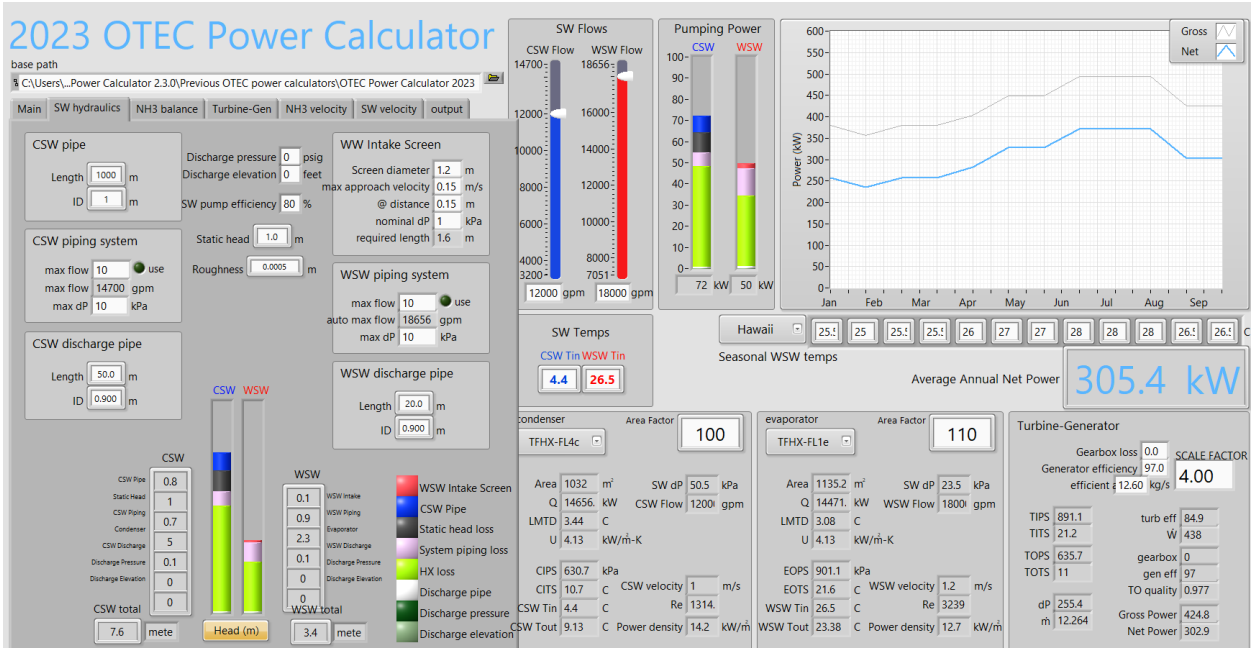

Figure 32. Baseline 300-kW OTEC system design.

For the same heat exchanger area, FL-1 has the highest net power/m^3 (Figure 33). The 4.24-mm plate spacing units (FL-3, FL-6, and FL-8) had the highest kW/m^2, but required up to 2X increase in warm seawater volumetric flow rate (Figure 34).

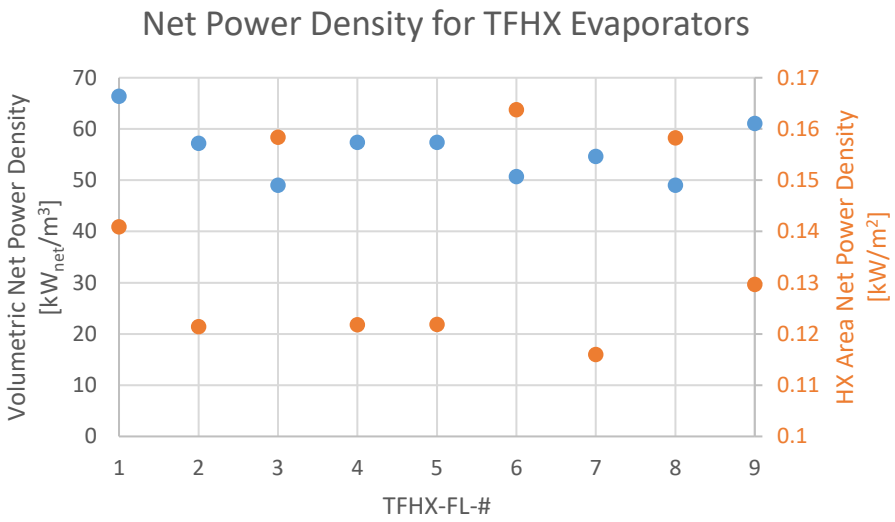

Figure 33. Comparison of net power density for different TFHX evaporators.

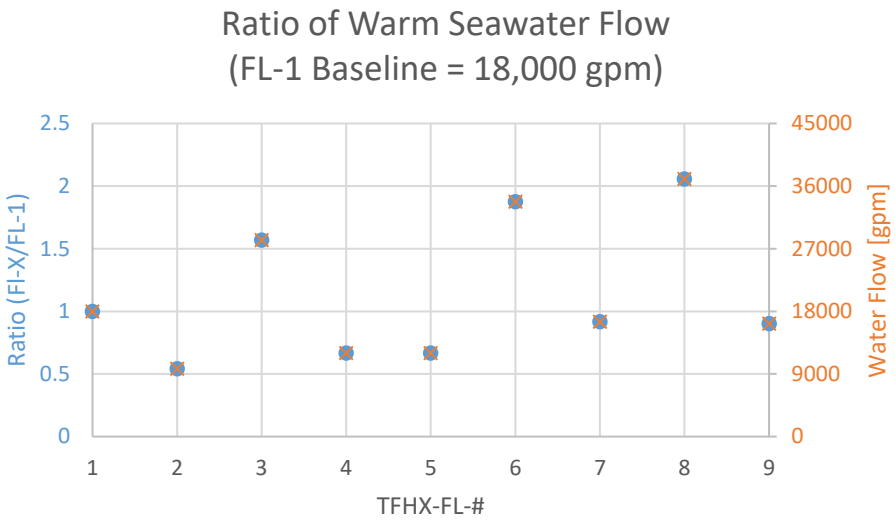

Figure 34. Ratio of optimized warm seawater flow rate compared to baseline TFHX-FL-1.

The same analysis was repeated by using FL-1 as an evaporator and varying the condenser design and cold seawater flow rate (for the same cold water pipe size). For the same heat exchanger area, FL-7 and FL-4 had the highest net power density (Figure 35). Unlike in the evaporator where there was no penalty in increasing the water flow rate, the 4.24-mm plate spacing designs (FL-3 and FL-6) suffered due to increased losses in the cold water pipe. With a larger cold water pipe, FL-3 and FL-6 may become more favorable and yield higher net power densities per heat exchanger area.

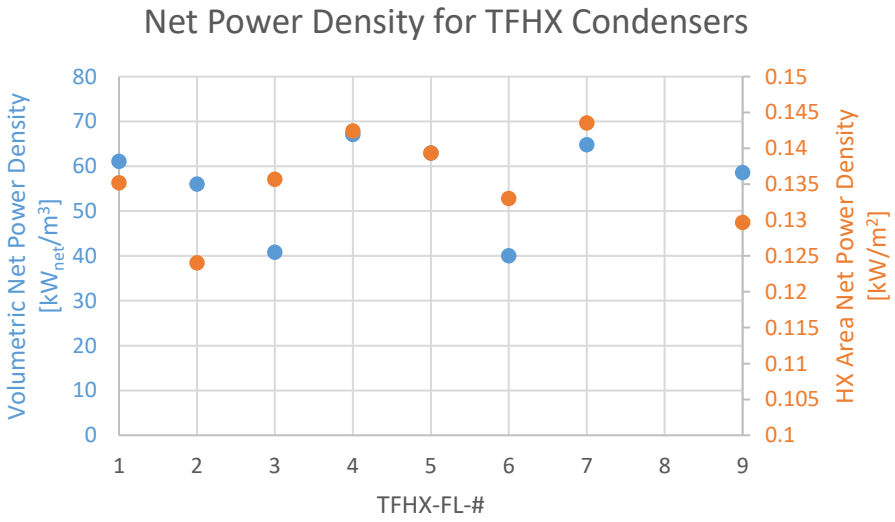

Figure 35. Comparison of net power density for different TFHX condensers.

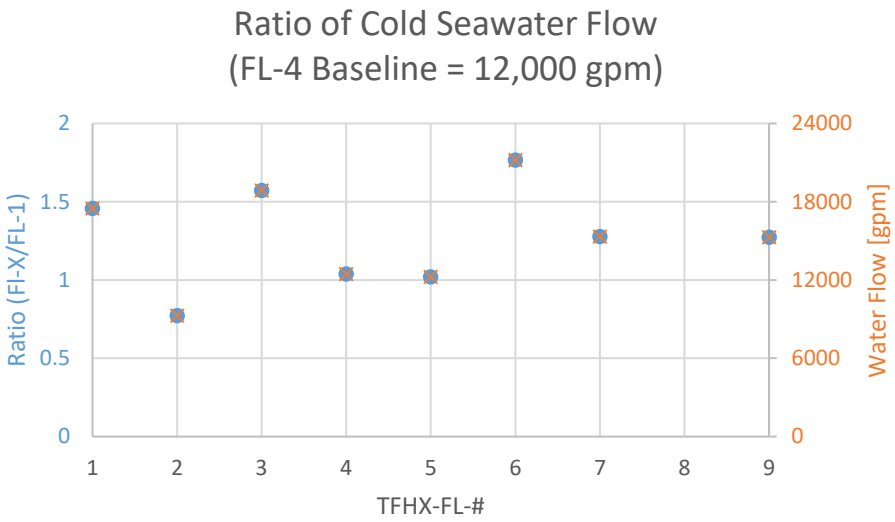

Figure 36. Ratio of optimized warm seawater flow rate compared to baseline TFHX-FL-4.

The results from the OTEC Power calculator are geared towards performance considerations; operational considerations, such as biofouling mitigation must also be considered when choosing an OTEC design.

5. TFHX CHARACTERIZATION

Supported and unsupported burst pressures are used to establish the pressure rating and predicted lifetime of a heat exchanger. In this period, Makai focused was on investigating steps to improve fatigue life and establishing an S-N curve for a single pattern design.

5.1.1. Cyclic Pressure Testing

Makai previously observed an additional step in fabrication improved fatigue life and developed a test plan to quantify the improvement in fatigue life. Four weld designs were selected (Table 4) and five parameters for the extra step for each design were tested. Each test required at least 3 plates to verify results were repeatable. A total of fifteen plates per design, 60 plates in total, were tested from 60-160 psig in the cyclic pressure tester. For clarity, the average cycles to failure is shown in figures in this section, not individual data points from each sample tested.

Table 4. Fatigue Test Plan – Weld Designs

Design	Supported Burst Pressure [psig]	Un-supported Burst Pressure [psig]	Effective Height [mm]
1	520	436	0.652
2	590	515	0.619
3	524	415	0.632
4	367	289	0.845

Up to 4X improvement in fatigue life was observed depending on parameter selection.

Finally, Makai began to construct an S-N curve for Design 1. The first two S-N curves for r=0 and r=0.375 are complete (Figure 37). (The r value indicates the minimum pressure divided by the maximum pressure.) The S-N curve can be used to predict the fatigue life of a design under different cyclic pressure amplitudes (maximum pressure – average pressure) for the same r-value.

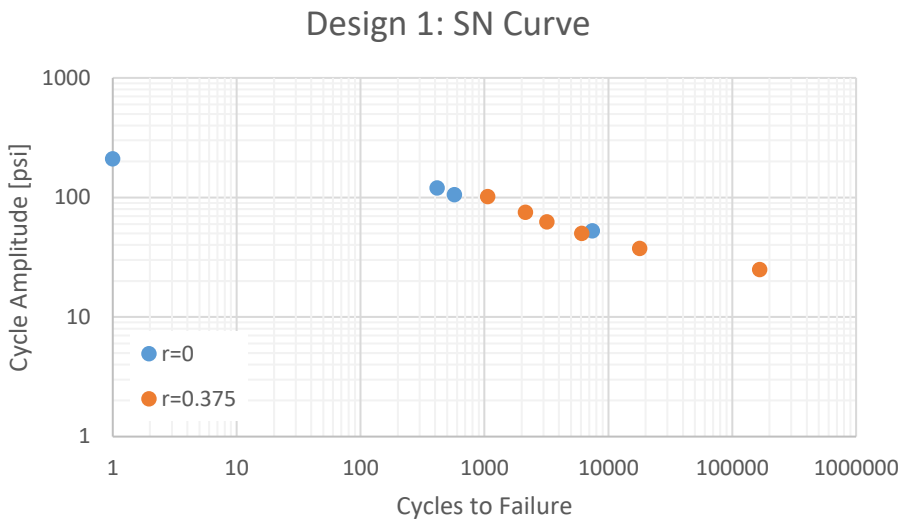

Figure 37. Design 1 SN curve.

A next step will be to perform the S-N curve for a set of plates re-expanded to 85% and confirm the improvement in fatigue life are consistent through the range of the S-N curve.

6. BIOFOULING

Untreated, biofouling can have a detrimental impact on heat exchanger performance by increasing the pressure drop through the heat exchanger and decreasing the heat transfer performance. Makai previously constructed a biofouling test station and completed a baseline test using FL-1. In this period, Makai evaluated a commercially available biofouling mitigation device called the Zeta Rod and constructed and began testing a prototype cleaning device.

6.1. ZETA ROD TESTING

The Zeta Rod operates on the theory of electrostatic dispersion of colloidal particles in a water system. It uses a ceramic rod and the walls of a metal pipe that houses the rod as two plates of a capacitor. Water flowing between the rod and pipe walls enters an electrostatic field created by the capacitor which reduces water surface tension and boosts the surface charge of particles and wetted surfaces; because of this surface charge, particles suspended in the fluid are repelled by other particles and from the wetted surfaces. The particles (including bacteria), do not aggregate or collected on wetted surfaces which prevents biofilm attachment and growth.

In December 2022, Makai received a Zeta Rod demonstration unit and modified the piping of the FL-1 slot in the Biofouling Test Station to install the Zeta rod (Figure 38).

Figure 38. Zeta Rod installed in FL-1 slot.

FL-1 plates were cleaned and re-used for the Zeta Rod test. An initial dP vs flow test was performed to establish a baseline curve and subsequent dP vs flow tests were performed every 30 days. Similar to the previous baseline test, cold seawater was flowing on the internal channels and

warm seawater was flowing in the external channels. In between dP vs flow tests, the warm seawater flow was maintained around 100 gpm. dP vs flow tests were conducted with maximum cold seawater flow and with seawater flows around 18 gpm. There was no direct measurement of cold seawater flow rates, so U-value comparisons have some error.

The inlet and outlet manifolds of both internal and external channels were inspected and cleaned every 30 days. There were occasional shells and debris in the warm seawater inlet manifold but no substantive growth or blockage was observed.

As observed in FL-1 baseline testing, little change in dP vs flow was observed for the first 30 days (Figure 39). At 60 days, the increase in dP at the same flow rate was ~25%. After 90 days, dP was about 1.8X compared to baseline at the same flow rate. U-value decreased ~10% between the Day 0 and Day 90 test (Figure 40).

Compared to the baseline FL-1 biofouling test, the Zeta Rod delayed the onset of pressure drop increased by about 3 weeks (Figure 41). For the same flow rate, the zeta rod test had similar dP at 63 days compared to 41 days in the baseline test.

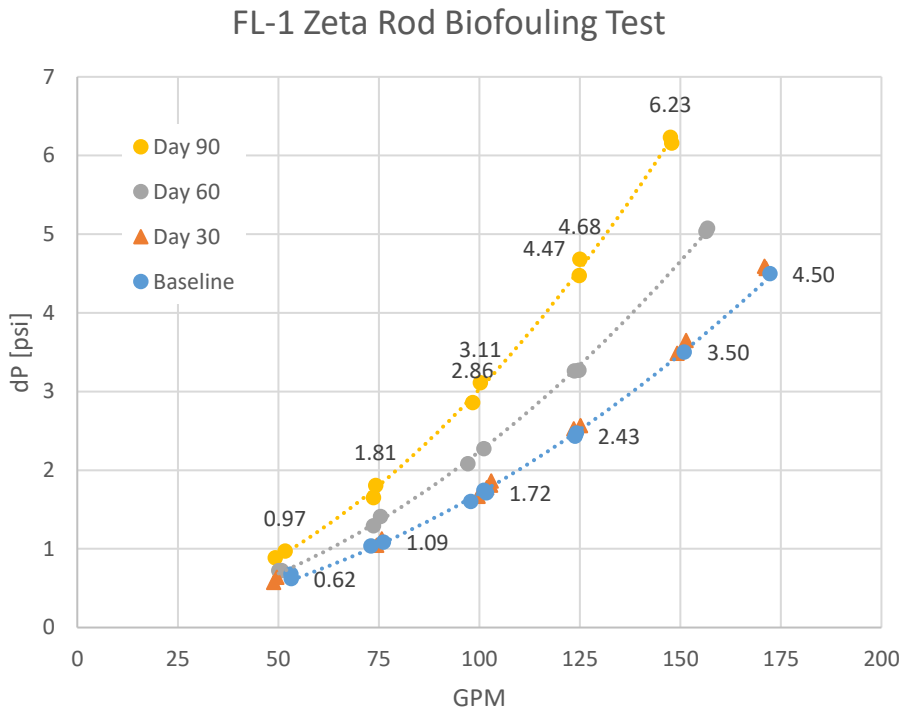

Figure 39. Zeta Rod test: Pressure drop vs flow.

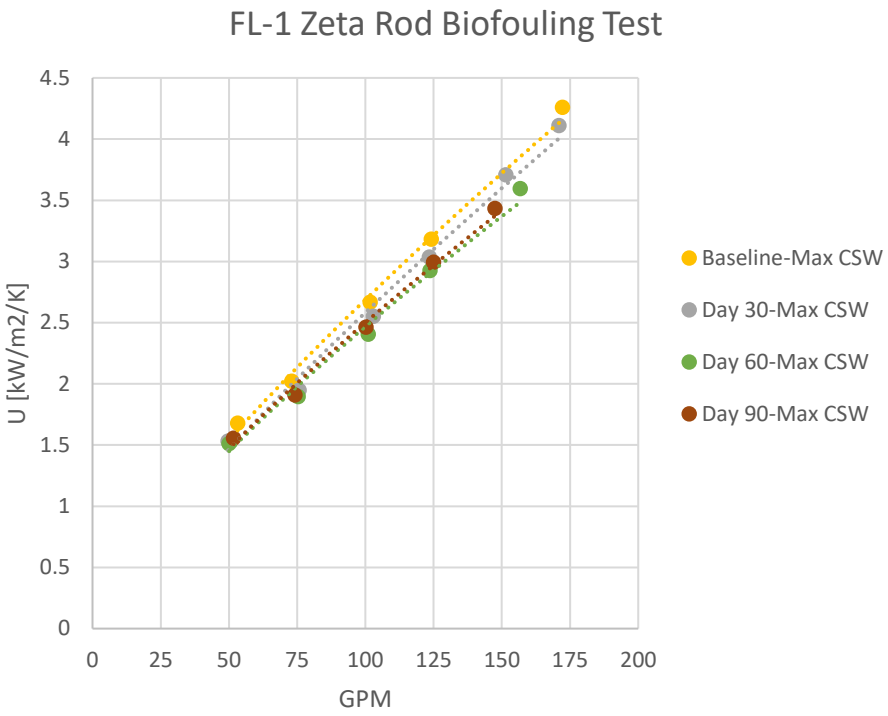

Figure 40. Zeta rod test: U-value vs flow.

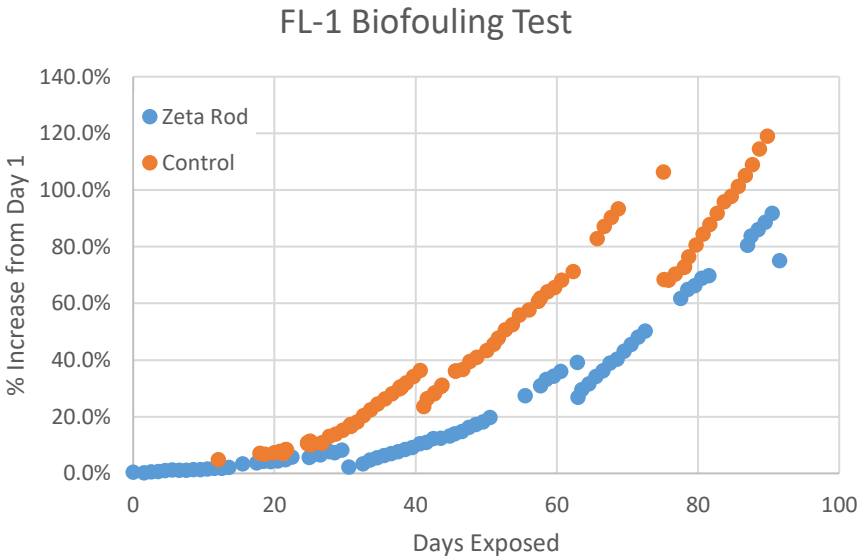

Figure 41. Comparison of zeta rod and baseline biofouling % increase in pressure drop relative to Day 0. Step-change drops in % increase are due to cleaning the manifolds.

6.2. CLEAN IN PLACE PROTOTYPE

The zeta rod delayed the onset of the effects of biofouling on performance but was not able to mitigate biofouling. Makai designed and constructed a prototype for a clean-in place mechanism.

In Makai's experience, mechanical brushing has been the most effective way of removing biofouling, but it is not practical to disassemble a heat exchanger unit every 3 months for cleaning. A mechanism that allows in situ cleaning would solve both biofouling issues and operational issues.

For the first iteration, Makai wanted to demonstrate it is possible to perform in situ brushing *and* that brushing is an effective cleaning method. A new housing was designed with an integrated brushing assembly. A new slot was added to the Biofouling Test station to test the prototype (Figure 42). A clear cover was installed so we could observe brushing efficacy, but the clear cover also provided direct sunlight and accelerated biofouling on the cover and the first plate.

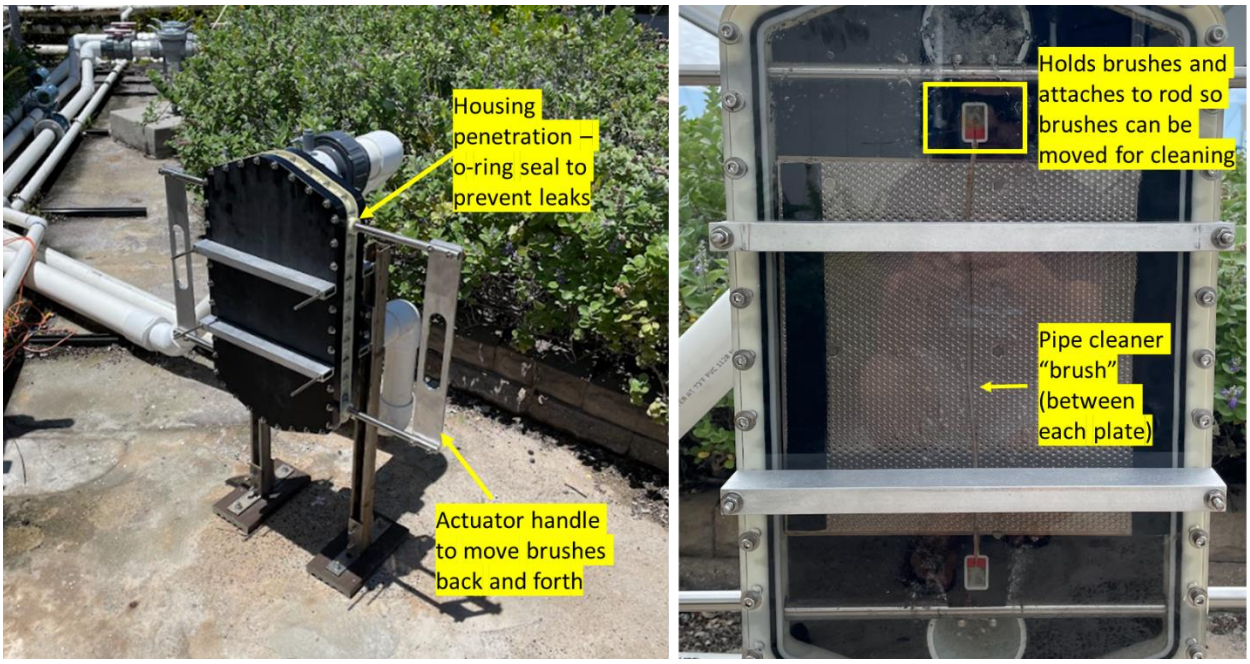

Figure 42. Clean in place prototype installed in Biofouling Test Station.

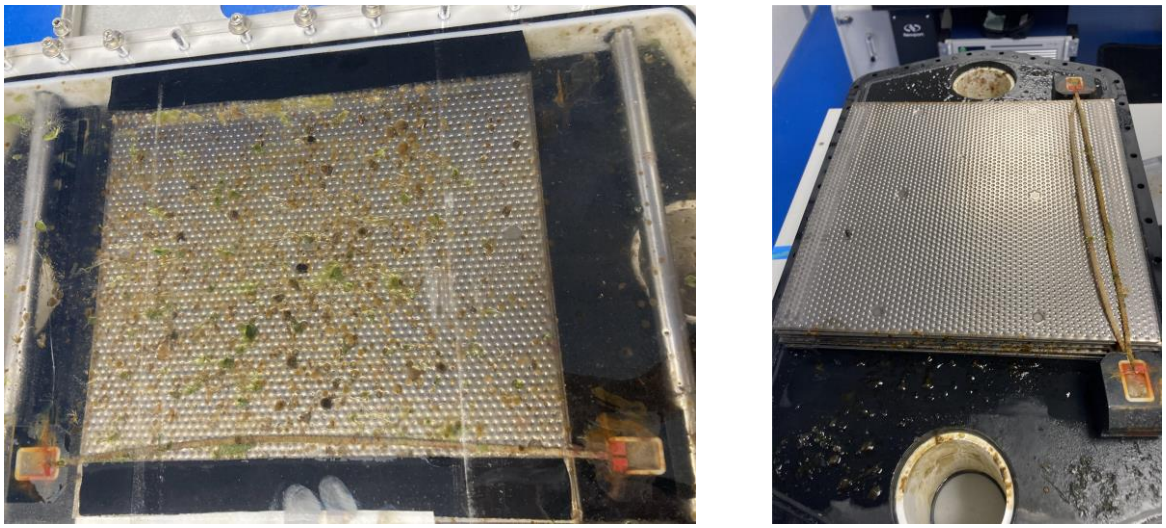

Figure 43. (left) Biofouling on the cover and first plate but not on the second plate (right).

The unit was manually cleaned every day during weekdays but not on weekends. The actuator was very difficult to move; a design modification will eventually be required so a motor can be used to move the brushes. In between flow tests, the external flow rate was maintained at ~ 10 gpm.

After 30 days, there was ~25% increase in pressure drop from the Day 0 data, however, the location of the brushes during the test was not recorded and there may be some discrepancy if the brushes aren't in the same location for each test.

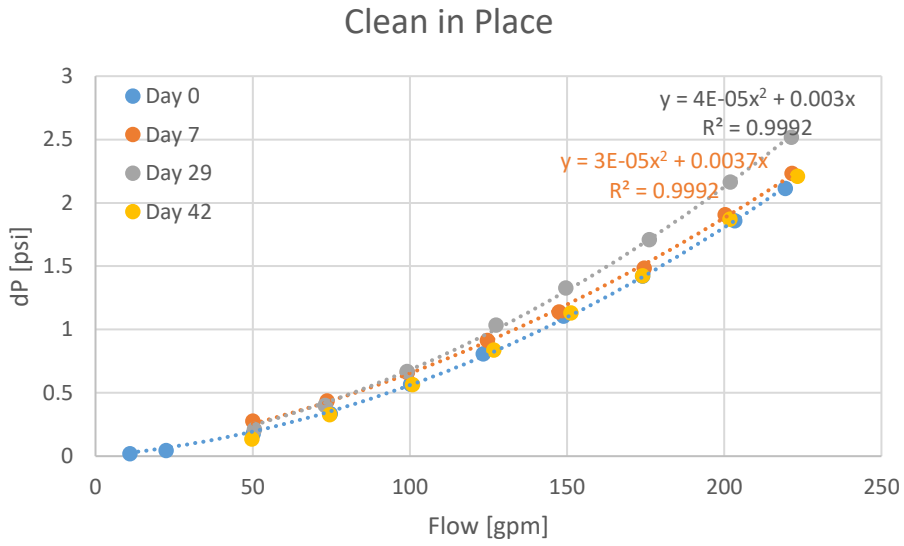

Figure 44. Pressure drop test for clean-in-place prototype.

With a 25% increase in pressure drop after 30 days, lining up with FL-1 baseline (no treatment) performance, it appeared the brushes were not effective at cleaning. However, once the unit was disassembled, except for the plate exposed to sunlight, there was little to no biofouling on the remaining plates. Several of the pipe cleaner brushes had broken loose on one end (but was still trapped between plates). The pipe cleaners were also rusty and some plates were discolored from rust (Figure 59). Upon inspection, the brushing appeared effective and Makai replaced all the pipe cleaners and re-assembled the unit to continue testing. This time, a heavy cover was placed over the unit to reduce direct sunlight exposure. After 1 week in water the pipe cleaners began to rust again.

A pressure drop vs flow test performed 5 days after re-installation (42 days after start of the initial test), shows the data align with the original measurements. Makai will continue to perform manual daily cleanings on weekdays and pressure drop vs flow tests every 2 weeks.

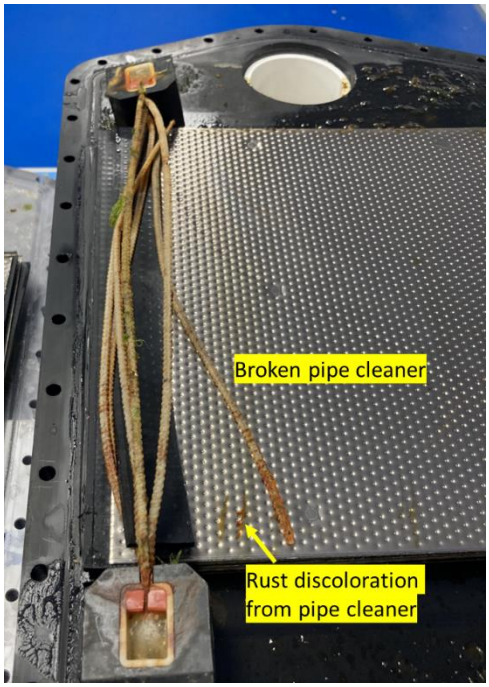

Figure 45. Broken pipe cleaner and rust stains on plates.

7. SUMMARY

Between August 2022 – May 2023, Makai made significant progress in improving TFHX plate fabrication success rate, performance testing additional full-length TFHX units, designing two new TFHX models, and prototyping new biofouling mitigation methods.

TFHX Design and Characterization. Makai developed two new TFHX designs, a pass-thru design for use as a seawater air conditioning unit (TFAC) and an enclosed water-water design (TFPX), also for SWAC or other cooling applications. Prototype units of each design were constructed and performance tested.

The existing four-port, full-length TFHX design experience a setback related to external fluid pressure rating. Initially designed for 50 psig pressure rating (100 psig burst pressure with a 2X safety factor), Makai tested two modules and both failed around 50 psig. This means the external fluid pressure rating must be lowered to 25 psig, which limits potential applications.

Finally, in cyclic pressure testing, Makai found parameters for an added step in fabrication that can lead to a 3X increase in cycles prior to failure. Makai was also able to complete two S-N curves for one pattern design.

TFHX Fabrication. Makai's on-going priority has been to improve plate fabrication success rate. In this period, Makai vetted and implemented machine vision/machine learning to automatically detect and repair pattern weld defects. Work is on-going to develop the algorithm to repair other weld types and to repair formed plates.

TFHX Performance Testing. In this period, Makai tested one air-water TFAC unit, one water-water TFPX unit, and seven ammonia-seawater (OTEC) four-port TFHXs. The TFAC could meet the performance requirements for the initial air-cooling application, but neither BOM nor NELHA are actively pursuing switching over to the TFAC (other internal priorities).

A 6" TFPX prototype was constructed as proof-of-concept and had comparable performance to previously tested mid-length INT units. This was somewhat surprising because eliminating the two 90° turns in the external fluid flow path should have lowered the pressure drop. The ability to remove/install plates without unstacking can be an advantage over plate-frame heat exchangers. Makai will continue to pursue suitable applications for the TFPX.

Finally, in OTEC testing, Makai has been using the OTEC Power Calculator to evaluate the different TFHX designs. The OTEC Power Calculator places each design in the context of an OTEC power plant and evaluates heat exchanger performance along with the effects of parasitic losses on the system.

Currently, FL-4 and FL-7 are the best performing condensers and FL-1 is the best performing evaporator in terms of volumetric net power density. For a condenser, TFHX designs with larger plate spacings are penalized in an OTEC system because of the parasitic losses in the cold water pipe. For an evaporator, there is no penalty in parasitic losses for TFHX designs with larger plate spacings, but the overall size of the OTEC system (volume) must be larger. However, there is also the issue of biofouling mitigation to consider when selecting the evaporator design. Larger plate

spacings may be easier to clean and ultimately lead to higher performance because the heat transfer surfaces won't be fouled.

Biofouling. Makai tested the zeta rod, a commercially available biofouling mitigation device and compared the results to previous baseline (untreated) test. The zeta rod delayed the onset of pressure drop increase due to biofouling by ~3 weeks. However, at the end of the 90 day test, pressure drop had increased by 75% on-track to match the observed increase in baseline pressure drop. The zeta rod system was unable to mitigate biofouling related performance degradation.

Makai designed, built, and tested a prototype for in-situ manual brushing. The brushing concept has promise, inspection after 30 days showed no biofouling attachment on plates not exposed to direct sunlight. In contrast, the plate exposed to direct sunlight and the clear cover was covered in growth. The test is still promising although the brush design requires revision; Makai believes the brush elements are barely touching (or not touching) plate surfaces in some areas and was therefore unable to remove biofouling from the first plate.

Upcoming Work

The major points of focus for Makai's near-term work are to:

- Improve upon the machine vision and machine learning algorithms to automate all weld defect (seal weld and feature welds) identification and repair
- Design fixturing to enable repair on a completed plate
- Continue SW-NH3 performance testing to identify optimal OTEC design, and
- Continue to develop, prototype and test in-situ biofouling control/mitigation systems

8. APPENDIX A – TFHX PERFORMANCE TESTING

8.1. DATA ACQUISITION AND INSTRUMENTATION

A custom developed Labview-based program was used to collect data. The instruments (Table 5) output a 4-20 mA signal, proportional to the measurement, which was read using National Instruments' NI 9208 Analog Input modules. Measurements were sampled 10X a second, averaged, and recorded every second.

Table 5. Sensors Used in TFHX Performance Testing

Measurement	Model	Range	Accuracy
Seawater Flow Rate	Rosemount 8705 Mag Meter	0-300 gpm	0.25% of rate
Ammonia Vapor Flow Rate	Micromotion Coriolis CMFS075M	0.03-1.74 kg/s	0.25% of rate
Ammonia Liquid Flow Rate	Micromotion Coriolis CMFS075M	0.03-1.74 kg/s	0.25% of rate
Seawater Inlet/Outlet Temperatures (Seawater-Ammonia Testing)	IsoTech milliK	0-100 C	0.01 C
Seawater Inlet/Outlet Temperatures (Seawater-Seawater Testing)	Intempco MIST 55	0-50 C	0.1 C + 0.1% FS
Seawater Inlet/Outlet Pressure	GE UNIK5000	0-30 psia	0.25% FS*
Ammonia Inlet/Outlet Temperature	Intempco MIST 55	0-50 C	0.1 C + 0.1% FS
Ammonia Inlet/Outlet Pressure	GE UNIK5000	400-1100 kPa gauge	0.25% FS*

* Another +/- 0.5% FS due to temperature error band needs to be added to the stated static accuracy. In practice, the pressure sensors are accurate to +/- 1 kPa.

8.2. CALCULATED VALUES

Several values are calculated by the 100 kW control software in real time. These values are used in determining steady state operation and characterizing heat exchanger performance.

8.2.1. Fluid Properties

Seawater properties used in mass flow rate and duty calculations are summarized in Table 6.

Table 6. Seawater properties used in seawater calculations

	Condenser	Evaporator
Temperature	6 °C	26.5 °C
Salinity	34.7 ppt	34.7 ppt
Density	1027.3 kg/m^3	1022.8 kg/m^3
Kinematic Viscosity	1.53E-6 m^2/s	9.26E-07 m^2/s
Thermal Conductivity	0.580 W/m/K	0.609 W/m/K
Prandtl Number	10.815	6.224

Ammonia fluid properties are calculated at the measured temperature and pressure using REFPROP10.

8.2.2. Seawater Mass Flow Rate

Seawater mass flow rate is calculated from the measured volumetric flow rate:

$$\dot{m} = \frac{gpm}{15850.3\ {}^{gpm}/_{m^3/s}} \times \rho$$

The density of cold seawater is taken to be 1027.3 kg/m^3 and the density of warm seawater is taken to be 1022.8 kg/m^3.

8.2.3. LMTD

LMTD is a measure of the average temperature difference across the heat exchanger. It is used in the calculation of overall heat transfer coefficient, U. LMTD is calculated according to:

$$LMTD = \frac{(T_{wsw\ in} - T_{sat\ @\ EOPS}) - (T_{wsw\ out} - T_{sat\ @\ EOPS\ in})}{ln\frac{T_{wsw\ in} - T_{sat\ @\ EOPS}}{T_{wsw\ out} - T_{sat\ @\ EOPS}}} \text{ (evaporator)}$$

$$LMTD = \frac{(T_{sat\ @\ CIPS} - T_{csw\ in}) - \left(T_{T_{sat\ @\ CIPS}} - T_{csw\ out}\right)}{ln\frac{T_{sat\ @\ CIPS} - T_{csw\ in}}{T_{T_{sat\ @\ CIPS}} - T_{csw\ out}}} \text{ (condenser)}$$

8.2.4. Duty

Duty is a measure of the heat transferred between warm and cold seawater and is used in the calculation of overall heat transfer coefficient. Duty can be calculated based on eitherseawater or based on the ammonia. The equations used to calculate the duty are:

$$Duty_{evap} = \dot{m_{wsw}} * c_{p,wsw} * (T_{wsw\ in} - T_{wsw\ out})$$

$$Duty_{evap} = \dot{m_{NH3}} * (h_{out} - h_{in})$$

$$Duty_{cond} = \dot{m_{csw}} * c_{p,csw} * (T_{csw\ out} - T_{csw\ in})$$

$$Duty_{cond} = \dot{m_{NH3}} * (h_{in} - h\ \ )$$

$\dot{m}$ = mass flow rate [kg/s],

c_p = specific heat capacity of seawater [kJ/kg],

T = seawater temperature [C], and

h = enthalpy [kJ/kg].

8.2.5. Overall Heat Transfer Coefficient

The overall heat transfer coefficient, U, is a measure of the overall efficiency of a heat exchanger. It is calculated according to:

$$U = \frac{Duty}{LMTD * Area}$$

LMTD = log mean temperature difference [C]

Area = heat transfer area of the heat exchanger [m^2]

Both duty and LMTD directly impact the calculation of overall heat transfer coefficient. The duty used to calculate the heat transfer coefficient is the ammonia duty.

8.2.6. Convective Heat Transfer Coefficients

The overall heat transfer coefficient is a function of the convective and conductive heat transfer coefficients:

$$\frac{\mathbf{1}}{\boldsymbol{UA}} = \frac{\mathbf{1}}{\boldsymbol{h_{sw}A}} + \frac{\boldsymbol{t}}{\boldsymbol{k_{foil}A}} + \frac{\mathbf{1}}{\boldsymbol{h_{NH3}A}} \qquad \textit{Equation 8-1}$$

where

A = heat transfer area [m^2],

h_{csw} = internal seawater convective coefficient [kW/m^2C],

h_{wsw} = external seawater convective coefficient [kW/m^2C],

t = foil thickness [m], and

k_{foil} = thermal conductivity of titanium foil [kW/mC],

The heat transfer area for each component in Equation 8-1 is the same; Equation 8-1 reduces to:

$$\frac{\mathbf{1}}{\boldsymbol{U}} = \frac{\mathbf{1}}{\boldsymbol{h_{SW}}} + \frac{\boldsymbol{t}}{\boldsymbol{k_{foil}}} + \frac{\mathbf{1}}{\boldsymbol{h_{NH3}}} \qquad \textit{Equation 8-2}$$

1/U is calculated from the data as described in Section 8.2.5. t/k_{foil} is a constant based on the physical and thermodynamic properties of the foil.

In order to determine h_{csw}, h_{wsw}, or h_{NH3}, the internal and external heat transfer coefficients was assumed to be constant for a fixed seawater flow rate or energy density and independent from the other side. By holding seawater flow rate constant and changing the energy density and vice versa, a matrix of U-values for each combination of seawater flow rates and energy densities was generated. The entire set of equations was solved simultaneously using the method of constrained least squares.